Regular Article – Theoretical Physics

# Maximum mass and universal relations of rotating relativistic hybrid hadron-quark stars\*

Gabriele Bozzola<sup>1,a</sup>, Pedro L. Espino<sup>2,b</sup>, Collin D. Lewin<sup>1,c</sup>, and Vasileios Paschalidis<sup>1,2,d</sup>

<sup>1</sup> Department of Astronomy, University of Arizona, Tucson, AZ, USA

<sup>2</sup> Department of Physics, University of Arizona, Tucson, AZ, USA

Received: 29 April 2019 / Revised: 23 June 2019

Published online: 16 September 2019

© Società Italiana di Fisica / Springer-Verlag GmbH Germany, part of Springer Nature, 2019

Communicated by D. Blaschke

Abstract. We construct equilibrium models of uniformly and differentially rotating hybrid hadron-quark stars using equations of state (EOSs) with a first-order phase transition that gives rise to a third family of compact objects. We find that the ratio of the maximum possible mass of uniformly rotating configurations —the supramassive limit— to the Tolman-Oppenheimer-Volkoff (TOV) limit mass is not EOSindependent, and is between 1.15 and 1.31, in contrast with the value of 1.20 previously found for hadronic EOSs. Therefore, some of the constraints placed on the EOS from the observation of the gravitational wave event GW170817 do not apply to hadron-quark EOSs. However, the supramassive limit mass for the family of EOSs we treat is consistent with limits set by GW170817, strengthening the possibility of interpreting GW170817 with a hybrid hadron-quark EOS. We also find that along constant angular momentum sequences of uniformly rotating stars, the third family maximum and minimum mass models satisfy approximate EOS-independent relations, and the supramassive limit of the third family is approximately 16.5% larger than the third family TOV limit. For differentially rotating spheroidal stars, we find that a lower-limit on the maximum supportable rest mass is 123% more than the TOV limit rest mass. Finally, we verify that the recently discovered universal relations relating angular momentum, rest mass and gravitational mass for turning-point models hold for hybrid hadron-quark EOSs when uniform rotation is considered, but have a clear dependence on the degree of differential rotation.

#### 1 Introduction

The properties of the equation of state (EOS) of dense nuclear matter constitute an important open problem that brings together several different fields ranging from astrophysics and gravitation to particle and nuclear physics. While the EOS is understood up to nuclear saturation density  $\rho_0 \approx 2.7 \times 10^{15}\,\mathrm{g\,cm^{-3}}$  [1–3], the situation is less clear at super-nuclear densities, with several different models being possible (see, e.g. [3, 4]). Regimes of such high density are expected to occur in Nature in the cen-

tral regions of compact stars, where the density can reach up to several times  $\rho_0$ .

The EOS determines several of the macroscopic prop-

erties of compact stars, such as mass and radius, thus affecting observable quantities (for reviews, see [5–8]). For this reason, astronomical observation is one of the primary tools to probe the high-density end of the EOS (see, e.g., [9]). Recently, the detection of gravitational waves from a binary neutron star [10] (event GW170817), accompanied by electromagnetic counterparts (events GW170817-GBM, and AT2017gfo [10–15]) provided a wealth of information that, under certain assumptions, helped to place constraints on the EOS [16–27] (see also [28] for a review). Among the EOSs that are compatible with GW170817, there are those with a firstorder phase transition from hadronic to quark matter at densities larger than  $\rho_0$ , which can lead to the so-called third family of stable stars. The third family consists of objects that are more compact than white dwarfs and neutron stars. These stars are hybrid hadron-quark stars (or just hybrid stars), i.e., configurations with a quark core

<sup>\*</sup> Contribution to the Topical Issue "First joint gravitational wave and electromagnetic observations: Implications for nuclear and particle physics" edited by David Blaschke, Monica Colpi, Charles J. Horowitz, David Radice.

<sup>&</sup>lt;sup>a</sup> e-mail: gabrielebozzola@email.arizona.edu

b e-mail: pespino@email.arizona.edu

c e-mail: collinlewin@email.arizona.edu

d e-mail: vpaschal@email.arizona.edu

surrounded by a hadronic shell<sup>1</sup>. The third family has been studied for a long time [30–46], with several of these earlier works focusing on "twin stars", which are hybrid stars in the third family whose mass is in the same range as the mass of neutron stars, but have smaller radii. Interest in hybrid stars has recently increased due to GW170817, because GW170817 is also compatible with at least one component being a hybrid star as first pointed out in [47]. Subsequent studies also focused on prospects of future multimessenger detections of the merger of binary compact stars with hybrid hadron-quark EOSs (e.g., [26,48–56]).

Motivated by the fact that such hybrid stars are compatible with GW170817, in this paper we focus on improving our understanding of uniformly and differentially rotating hybrid stars. These have received only little consideration [36,39] and many of their properties are largely unexplored. We adopt the same EOSs with first-order phase transitions to quark matter introduced in [47], and focus on answering the following set of questions: What is the maximum mass for uniformly and differentially rotating hybrid stars? Are these compatible with constraints from GW170817? Do rotating hybrid stars satisfy the same existing universal relations that hadronic EOSs satisfy?

The maximum mass that a non-rotating relativistic star<sup>2</sup> can support —the TOV limit— is determined by the EOS. However, rotation can increase the maximum supportable mass [59–62]. In the case of hadronic EOSs, uniform rotation increases the maximum mass by about 20 [60,63–66]<sup>3</sup>. Equilibrium configurations whose mass exceeds the TOV limit are commonly referred to as "supramassive" [70]. The maximum mass supported when allowing for maximal uniform rotation is known as the "supramassive limit". Given the approximate EOS-independence (for hadronic EOSs), the supramassive limit has been used to place constraints on the TOV limit mass using observations (e.q. [20, 25]). Whether this universality for the ratio of the supramassive limit to the TOV limit mass holds for hybrid stars has not been investigated before and we test this here. Using the code of [70], we construct mass shedding sequences and find that for the hybrid EOSs we treat, this ratio is between 1.15 and 1.30. As a result, the universality does not hold for hybrid stars or, at least, the spread of the universality is significantly enhanced. However, using the same arguments as in [20, 25], we find that the supramassive limit of our hybrid EOSs is consistent with GW170817, lending further support to the results of [47] that GW170817 is compatible with hybrid hadron-quark EOSs.

Differential rotation can greatly boost the maximum mass that a star can have [65,71]. The term "hypermassive" [71] is used to describe those stars that are more

massive than the supramassive limit, and are supported by the additional centrifugal support provided by differential rotation. There also exist stars that can support more than two times the TOV limit mass (these were termed "ubermassive" in [72]), and which can arise only when differential rotation is present. Differential rotation plays an important role in temporarily stabilizing a binary neutron star merger remnant, and likely many merger remnants go trough a hypermassive phase (see, e.g., [62, 73, 74] for recent reviews on binary neutron star mergers). Differentially rotating stars have been shown to exhibit a rich and interesting solution space (see [75–77] for polytropes, [72] for hadronic EOSs, and [78, 79] for strange quark stars). For instance, as the degree of differential rotation varies, the topology of the star can change from spheroidal to quasi-toroidal, where the maximum energy density does not occur at the geometric center of the star, but in a ring around the stellar center of mass. Studies of the dynamical stability of such quasi-toroidal configuration are under way and it is found that these configurations are dynamically unstable [80]. For this reason, in this paper we focus primarily on the maximum mass that differentially rotating spheroidal hybrid star configurations can support using the differential rotation law of [81,82]. The motivation for this study is that quark deconfinement can happen not only for isolated stars, but also following a binary neutron star merger [53], that can result in a differentially rotating hybrid star. Using the code of [70], we find that a lower-limit on the maximum supportable rest mass is 123% more than the TOV limit rest mass. This means that ubermassive spheroidal hybrid hadron-quark configurations can exist.

In the context of binary mergers, EOS-independent relations have proven useful as tools to devise tests for general relativity and break degeneracies in gravitational wave signals. For instance, the universal I-Love-Q relations [83–86] were used in [22] to tighten the constraints placed on the tidal deformability of the two components of the GW170817 binary. In [47] it was verified that, for the EOSs we adopt here, the I-Love-Q relations are still satisfied with a spread of at most 3% in both slowly and rapidly rotating hybrid stars<sup>4</sup>. In [90], relations that do not depend on the EOS or the degree of differential rotation were found for turning-point models, which are the critical points of the gravitational mass along equilibrium sequences with fixed angular momentum or rest mass. For uniformly rotating configurations, turning points locate the onset of the unstable branch, and for this reason are useful to study the stability properties of rotating stars [91–94]. We verify that the universal relations

<sup>&</sup>lt;sup>1</sup> It is also possible for a fourth family to arise [29] if the EOS has an additional phase transition. However, this scenario will not be considered here.

 $<sup>^2</sup>$  We will interchangeably also use the terms "static" and "TOV" to indicate non-rotating stars [57,58].

<sup>&</sup>lt;sup>3</sup> However, it has been shown that strange quark-matter stars can support up to 40% more than the non-rotating limit [67–69].

 $<sup>^4</sup>$  In [87] different hadron-quark equations of state were adopted to investigate the I-Love-Q relations. The authors constructed sequences of uniformly rotating stars with constant angular velocity and reported that EOSs with a first-order phase transition violate the universality. However, the universal relations for rapidly spinning and slowly spinning stars are different, and "universality" is restored when considering sequences with constant  $J/M^2$  instead of constant angular frequency [88,89].

relating angular momentum, rest mass and gravitational mass for turning-point models found in [90] hold for hybrid hadron-quark EOSs when uniform rotation is considered, but have a clear, albeit weak, dependence on the degree of differential rotation.

The rest of the paper is structured as follows. In sect. 2 we review the EOSs we consider in this work. In sect. 3 we briefly describe the code we use to perform our study. In sect. 4 we compute the supramassive limit for hybrid stars and discuss its implications for GW170817. We also test the previously found universal relations of [66] and [90] for the maximum mass along constant angular momentum sequences, and point out that the minimum mass twin stars also satisfies a universal relation. In sect. 5 we compute the maximum rest mass of differentially rotating spheroidal hybrid stars, and test the dependence on the degree of differential rotation of the aforementioned universal relations. We conclude in sect. 6 with a summary of our main findings. Unless otherwise specified, throughout this paper we adopt geometrized units where c = G = 1(where c is the speed of light in vacuum and G the gravitational constant). Square brackets are used to designate the units of quantities. For instance,  $[M_{\odot}]$  indicates the solar mass. In addition, when we use the word "mass" we refer to the gravitational (Arnowitt-Deser-Misner, ADM) mass for which we use the symbol M (or  $M_{ADM}$ ) with other sub- or superscripts except for the subscript 0. We will specify "rest" or "baryon" mass otherwise, and to designate rest mass we use the subscript 0 with other sub- or superscripts, e.g.,  $M_0$ .

### 2 Equations of state

The hybrid hadron-quark EOSs we employ are the same as those developed in [47] for the EOSs introduced in [29] (Set I) and [46] (Set II). Here we briefly describe these EOSs, and refer the interested reader to [47] for more details. Note that we use a different naming convention compared to [47], and the map between the two is listed in table 1, where we also report the maximum mass for static stars in both the hadronic and third family branches.

The EOSs correspond to zero-temperature matter in beta-equilibrium with a low-density hadronic phase and a high-density quark phase that are matched through a first-order phase transition. High tension at the quark-hadron interface is assumed, leading to a sharp transition boundary between the two phases. A low-density crust component based on the model of [95,96] is also added to both sets of EOSs. In all EOS models the pressure matching between the two phases is performed via a Maxwell construction.

The Set I EOSs have a hadronic part that follows [97] in applying a covariant density functional theory [98] with density-dependent couplings [99]. The quark phase in Set I is described by a MIT bag model [100–103], adopting the constant sound speed  $(c_s)$  parametrization [29,104–106]. Hence, the Set I quark phase pressure P as a function of

Table 1. Labels of the equations of state employed in this paper and their corresponding labels in [47]. EOSs T1–TT belong to Set I and have a first-order phase transition with energy-density jump parametrized by  $\xi$  as shown in eq. (2). Their quark phase is described by eq. (1). On the other hand, EOSs A4–A7 belong to Set II, and have a quark phase parametrized as piecewise polytropes as shown in eq. (3). We also report the maximum mass that a TOV star can have on the hadronic  $(M_{\text{Max},\text{hadronic}}^{\text{TOV}})$  and the hybrid  $(M_{\text{Max},\text{hybrid}}^{\text{TOV}})$  branches, respectively.

EOS	EOS in [47]	$M_{ m Max,hadronic}^{ m TOV}$	$M_{ m Max,hybrid}^{ m TOV}$
		$[M_{\odot}]$	$[M_{\odot}]$
Т1	ACS-I $\xi = 0.10$	2.00	2.47
T2	ACS-I $\xi=0.27$	2.00	2.31
T4	ACS-I $\xi = 0.43$	2.00	2.17
Т6	ACS-I $\xi = 0.60$	2.00	2.05
T7	ACS-II $\xi = 0.70$	1.50	2.14
T8	ACS-II $\xi = 0.80$	1.50	2.08
T9	ACS-II $\xi = 0.90$	1.50	2.02
TT	ACS-II $\xi = 1.00$	1.50	1.98
A4	ACB4	2.01	2.11
A5	ACB5	1.40	2.00
A6	ACB6	2.01	2.00
A7	ACB7	1.50	2.00

the energy density  $\epsilon$  is given by

$$P(\epsilon) = \begin{cases} P_{\text{tr}} & \epsilon_1 \le \epsilon \le \epsilon_2, \\ P_{\text{tr}} + c_s^2(\epsilon - \epsilon_2) & \epsilon \ge \epsilon_2, \end{cases}$$
 (1)

with  $P_{\rm tr}$  value of the pressure at the phase transition (which occurs in the energy density range  $\epsilon_1 \leq \epsilon \leq \epsilon_2$ ). The energy density jump is parametrized by the value of  $\xi$  defined through<sup>5</sup>

$$\epsilon_2 = (1 + \xi)\epsilon_1. \tag{2}$$

The values of  $\epsilon_1, \xi, P_{\rm tr}$  and  $c_s$  that produce the Set I EOSs (labeled here T1–T9 and TT) are listed in table I of [47].

Set II [46] consists of a piecewise polytropic representation [6,107,108] of the quark phase in which the pressure is

$$P(n) = K_i \left(\frac{n}{n_0}\right)^{\Gamma_i} \quad \text{for } n_i < n < n_{i+1}, \qquad (3)$$

where n is the baryon number density and  $n_0$  its value at the nuclear saturation density and  $K_i$  the polytropic constant. The second polytrope has  $\Gamma_2 = 0$  so that the pressure is constant, corresponding to the phase transition. The various coefficients that specify these EOSs (labeled here as A4–A7) are listed in table II of [47]. Note that EOSs with similar properties as the EOSs in Set I and II have been obtained recently within a relativistic density

<sup>&</sup>lt;sup>5</sup> In [47] the letter j is used instead of  $\xi$ .

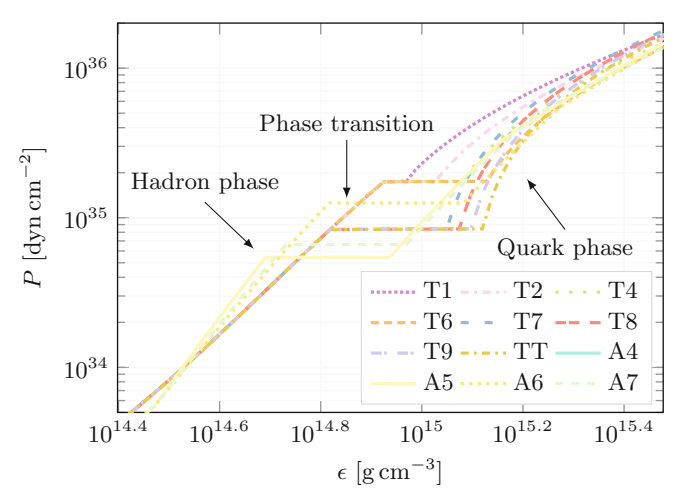


**Fig. 1.** Pressure P as a function of the energy density  $\epsilon$  for the equations of state studied in this paper.

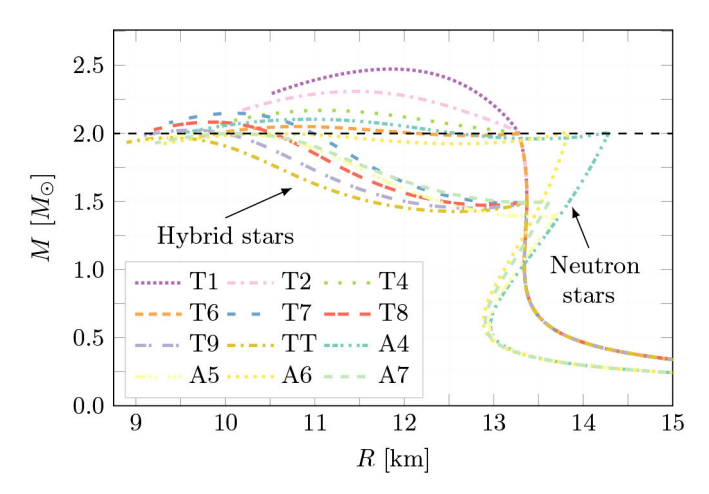


Fig. 2. Mass-radius relation for non-rotating stars with the EOSs listed in table 1 and plotted in fig. 1. Equations of state with quark-hadron transitions allow for a third family of relativistic stars more compact than neutron stars, and hence hybrid stars are on the left part of the curve. The hadronic and/or the hybrid branches of all the EOSs lead to configurations (at least marginally) compatible with the constraint of a  $2 \, M_{\odot}$  pulsar (dashed line).

functional approach to quark matter [36, 41, 109]. Moreover, in [56], equations of state like the ones considered here are systematically explored to find the parameters for the phase transition allowed by GW170817 and to characterize the properties of non-rotating stars constructed with such EOSs.

Figure 1 shows the pressure P as a function of the energy density  $\epsilon$  for the different EOSs, and fig. 2 depicts the resulting mass-areal radius relationship for non-rotating compact stars. The EOSs are compatible with the observational constraint of a pulsar mass of  $(1.97\pm0.04)\,M_\odot$  [110–113], and half of them are also compatible with the newly discovered  $2.17^{+0.11}_{-0.10}\,M_\odot$  pulsar J0740+6620 [114]. The EOSs span a relatively large range of compactness and radii (10–13.5 km), and as such allow us to test for univer-

sal relations. Despite the fact that some of the EOSs in our sample are incompatible with J0740+6620, we include them in our study to check whether existing universal relations are respected independently of the EOS.

#### 3 Methods

We assume that neutron star matter can be described as a perfect fluid with no meridional currents. An equilibrium model for a rotating general-relativistic star is a stationary and axisymmetric solution of Einstein's equations coupled with the equation of hydrostationary equilibrium. Under these assumptions, the fluid four-velocity is given by

$$u = (u^t, 0, 0, u^{\phi}), \tag{4}$$

and the line element  $ds^2$  of the spacetime is

$$ds^{2} = -e^{\gamma+\rho}dt^{2} + e^{\gamma-\rho}r^{2}\sin^{2}\theta(d\phi - \omega dt)^{2}$$
  
+  $e^{2\alpha}(dr^{2} + r^{2}d\theta^{2}),$  (5)

with  $(t, r, \theta, \phi)$  quasi-isotropic coordinates, and  $\gamma$ ,  $\rho$ ,  $\alpha$ ,  $\omega$  spacetime potentials that depend on the coordinates r,  $\theta$  only [62, 115, 116].

To solve the equilibrium equations, an EOS and a rotation law have to be supplied (see [62] for a recent review on theoretical and numerical approaches to the construction of rotating relativistic stars). For uniform rotation, we fix  $\Omega = u^\phi/u^t$  (the local angular velocity of the fluid as seen by an observer at rest at infinity) to be constant. For differential rotation, we adopt the Komatsu-Eriguchi-Hachisu (KEH) j-constant law [81,82], which is described by

$$u^t u_\phi = A^2 (\Omega_c - \Omega), \tag{6}$$

where  $\Omega_c$  is the angular velocity evaluated on the rotation axis, and A is a parameter with units of length that determines the lengthscale of variation of angular velocity within the star. This rotation law is not the only possible choice, but it is most commonly studied due to its simplicity (for a summary of other differential rotation laws, see [62]). In the following, instead of using A, we work with the dimensionless parameter  $\hat{A}^{-1}$  defined by

$$\hat{A}^{-1} = \frac{r_e}{A} \,, \tag{7}$$

where  $r_e$  is the coordinate radius of the star at the equator. Stars with  $\hat{A}^{-1}=0$  are uniformly rotating.

We use the code developed in [60, 63] (the "Cook code") to solve the structure equations and construct equilibrium models for rotating stars. For a given EOS and degree of differential rotation  $\hat{A}^{-1}$ , a rotating equilibrium model is built by providing the maximum energy density  $\epsilon_{\text{max}}$  and the ratio of the polar  $(r_p)$  to equatorial coordinate radius  $r_e$ . In the case of differential rotation with the KEH law, the set of parameters  $\{\epsilon_{\text{max}}, r_p/r_e, \hat{A}^{-1}\}$  does not uniquely specify an equilibrium model, in spite of the

fact that it is sufficient to find a solution [75]. To distinguish between physically distinct models that have the same  $\{\epsilon_{\max}, r_p/r_e, \hat{A}^{-1}\}$ , the parameter

$$\beta = -\left(\frac{r_e}{r_p}\right)^2 \frac{\mathrm{d}(z^2)}{\mathrm{d}(\varpi^2)}\Big|_{\varpi=r_e} \tag{8}$$

was introduced in [75]. Here  $\varpi = r \sin(\theta)$  and  $z = r \cos(\theta)$  are cylindrical coordinates, and the derivative is evaluated on the surface of the star at the equator. In practice, it is more convenient to work with a new quantity  $\hat{\beta}$  defined in terms of  $\beta$  as

$$\hat{\beta} = \frac{\beta}{1+\beta} \,. \tag{9}$$

The parameter  $\hat{\beta}$  describes how close to the mass-shedding limit a configuration is, and approaches three limiting values according to the stellar shape in the solution space: in the case of a spherical solution,  $\beta=1$  and so  $\hat{\beta}$  is 1/2; for a model close to the mass-shedding limit, the stellar surface is highly pinched near the equator, which implies that the derivative appearing in eq. (8) vanishes, and hence  $\hat{\beta}$  approaches 0; finally, for a quasi-toroidal shape the ratio  $r_p/r_e$  becomes very small, and hence  $\beta$  becomes large. In this limit  $\hat{\beta}$  approaches 1.

In the case of the KEH rotation law, the solution space of differentially rotating stars is fully specifiable by the quadruplet of parameters  $\{\epsilon_{\max}, r_p/r_e, \hat{A}^{-1}, \hat{\beta}\}$  [75]. Our code does not have the capability of fixing  $\hat{\beta}$  directly, but, as in [72], we produce models with different values of  $\hat{\beta}$  given the other parameters  $\{\epsilon_{\max}, r_p/r_e, \hat{A}^{-1}\}$  by following specific trajectories in the parameter space. This is especially relevant for our discussion in appendix A, where we study the different solution types for hybrid stars.

#### 4 Uniform rotation

In this section we focus on the case of uniform rotation. We compute the supramassive limit mass and the maximum mass on sequences of constant angular momentum, and test the applicability of the universal relations found in [66] and [90] to the hybrid hadron-quark EOSs listed in table 1. Differential rotation is treated in sect. 5.

One of the most important macroscopic parameters related to an equation of state is the maximum mass that an equilibrium rotating star can support<sup>6</sup>. To study supramassive hybrid stars we construct equilibrium sequences with constant angular momentum J. For these computations, we set the angular resolution of the Cook code to 300 points, the radial to 500 and used a basis of 20 Legendre polynomials. Then, each sequence is constructed with at least 500 models logarithmically equispaced in the central energy density. Examples of such sequences are depicted in fig. 3 for EOS T9, where boxes indicate the stars with

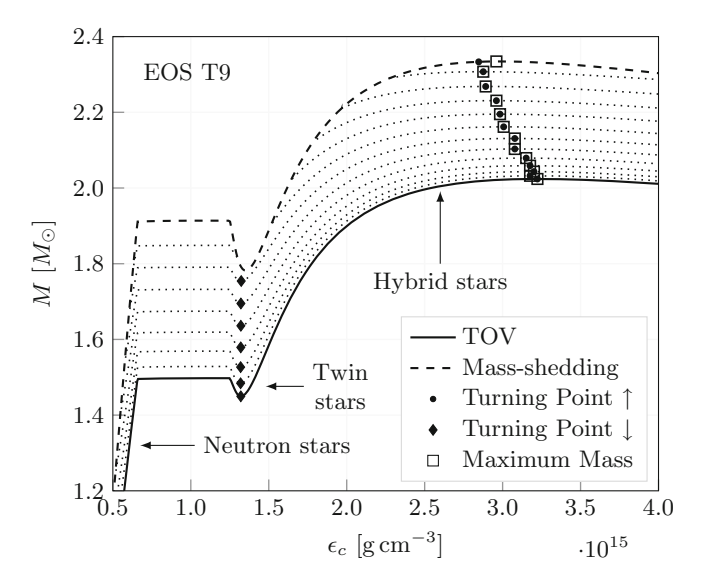


Fig. 3. Constant angular momentum equilibrium sequences for uniformly rotating stars with EOS T9. The black solid line is the non-rotating sequence, and the dashed line represents the mass-shedding sequence. Black filled circles indicate the top turning points, whereas boxes are models with maximum mass along the sequence. Diamonds designate the bottom turning points, which indicate the least massive twin star. Most of the turning points lie inside a box because they are also the most massive model along the sequence. The flat region that occurs in the density range  $\epsilon_c \in (0.6, 1.4) \, 10^{15} \, \mathrm{g \, cm^{-3}}$  is a direct consequence of the one in fig. 1: multiple values of  $\epsilon_c$  lead to the same central pressure, which in turn results in models with the same mass.

maximum mass along each J-constant sequence. In fig. 3, we also highlight other notable models: the  $turning\ points$  indicated with filled diamonds and filled circles. In fig. 3, most of the circles lie inside a box, since those turning points are also the most massive model of the sequence.

Given a sequence of equilibrium models with constant angular momentum J, and varying central energy density  $\epsilon_c$ , the turning points are the stationary points of the function  $M(\epsilon_c)$ , where  $M(\epsilon_c)$  is the gravitational mass along the sequence. For a constant J sequence, a turning point is defined by the condition

$$\left. \frac{\partial M(\epsilon_c)}{\partial \epsilon_c} \right|_I = 0. \tag{10}$$

For constant angular momentum sequences and hadronic EOSs, the turning points are local maxima, whereas for constant  $M_0$  sequences the turning points are local minima. By virtue of the turning point theorem [91,117] that applies to uniformly rotating configurations, the turning-point lines for J-constant sequences coincide with those of  $M_0$ -constant sequences. In this work we located the turning points along J-constant sequences by interpolating with a cubic spline around the local maxima and minima model of the sequence, and then finding the roots of the derivative of the cubic spline interpolant.

<sup>&</sup>lt;sup>6</sup> The most massive models are typically dynamically unstable [91,92,94]. In this paper we ignore the issue of stability and focus on constructing equilibrium models.

In the case of EOSs exhibiting a hadron-quark phase transition with a large jump in energy density, typically each J-constant sequence has multiple turning points. In this paper we focus on the two turning points of Jconstant sequences that occur at central energy densities higher than the phase-transition. We call them "top" (labeled with an upward pointing arrow ↑) and "bottom" (labeled with a downward pointing  $\downarrow$ ), indicating the higher and lower mass turning point, respectively. In all figures diamonds represent bottom turning points, filled circles indicate top turning points, and boxes designate the most massive models. Top turning-point models are interesting because for uniformly rotating stars they detect the onset of the instability to collapse [91, 92]. On the other hand, bottom turning points indicate the least massive twin star which must be unstable, too. Not all EOSs in our set have bottom turning points: T1, T2 and T4 have too small a jump  $\xi$  to produce such configurations (as can be seen in fig. 2, where these three EOSs do not undergo a dip above the phase transition energy density). These EOSs do not exhibit twin star solutions.

The TOV sequences are constant angular momentum (J=0) sequences. Their top turning points indicate the maximum mass allowed for static configurations<sup>7</sup>, and their bottom turning points indicate the minimum mass of non-rotating twin stars. These maximum and minimum masses provide fundamental mass scales associated with each EOS, and will be used to normalize other quantities. We will append the superscript "TOV" to designate these mass, so that  $M_{\rm Max}^{\rm TOV}$  and  $M_{0,{\rm Max}}^{\rm TOV}$  are the maximum gravitational and baryonic mass of a non-rotating hybrid star in the third family, respectively, whereas  $M_{0,{\rm V}}^{\rm TOV}$  and  $M_{0,{\rm V}}^{\rm TOV}$  are the minimum gravitational and rest mass for a static twin star<sup>8</sup>.

## 4.1 The supramassive limit

An EOS-insensitive relation for hadronic EOSs that relates the maximum mass  $(M_{\text{Max}})$  and angular momentum along J-constant sequences was recently found in [66]. The resulting universal relation (eq. (12) in [66]) is expressed in terms of J normalized to the maximum possible angular momentum  $J_{\text{Max}}$  that can be achieved with uniform rotation, and is the following

$$\frac{M_{\uparrow}}{M_{\rm Max}^{\rm TOV}} = 1 + 0.1316 \left(\frac{J}{J_{\rm Max}}\right)^2 + 0.0711 \left(\frac{J}{J_{\rm Max}}\right)^4. \eqno(11)$$

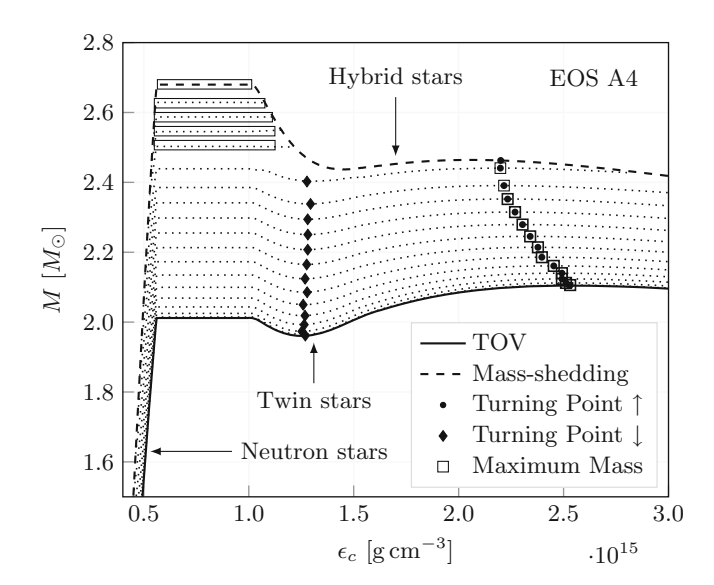


**Fig. 4.** Same as fig. 3, but for EOS A4. Rotation leads to a relative increase in the mass which is larger when the central energy density is in the phase-transition region. For values of  $\epsilon_c$  in this range, a star can be spun up at higher values of the angular momentum, increasing the supramassive limit. The flat branches at high angular momentum have models with the same mass, for this reason, each of those stars is a maximum-mass model (empty rectangles).

This last equation can be used to estimate the supramassive limit for hadronic EOSs, and yields the approximately EOS-independent value of 20% larger than the TOV limit. Here we are interested in testing whether eq. (11) applies to hybrid hadron-quark EOSs. Moreover, we explore whether a similar relation exists for hybrid EOSs not only for the top turning points, but also for the bottom ones. As a reminder, we note that for hybrid EOSs, the top turning point is not necessarily the most massive model along a J-constant sequence, as shown for example in fig. 4.

## 4.1.1 Maximum mass

In fig. 5 we plot the maximum possible gravitational mass normalized to  $M_{\rm Max}^{\rm TOV}$  on J-constant sequences as a function of J normalized to  $J_{\rm Max}^{\rm supra}$ , the angular momentum of the most massive uniformly rotating star i.e., the supramassive limit configuration. This choice ensures that the maximum mass is reached when  $J/J_{\rm Max}^{\rm supra}=1$ . As is clear from fig. 5, some of the EOSs in our set produce uniformly rotating stars that can support more mass than  $1.20\,M_{\rm Max}^{\rm TOV}$ . On the other hand, some EOSs cannot even reach such a large enhancement in mass compared to the TOV limit mass. To be more specific, the supramassive limit mass varies from  $1.15\,M_{\rm Max}^{\rm TOV}$  for TT to  $1.31\,M_{\rm Max}^{\rm TOV}$  for A6.

#### 4.1.2 Implications for GW170817

In [20,25] the result that for hadronic EOSs the ratio of the supramassive limit to the TOV limit is EOS-independent

<sup>&</sup>lt;sup>7</sup> This is not true for EOS A6, since, for this EOS, non-rotating stars with central energy density within the phase transition have mass  $M=2.01\,M_{\odot}$ , whereas the top turning point has mass  $M=2.00\,M_{\odot}$ . Since our focus is on the stable branch of the third family of stars, the top turning point is the maximum mass of the third family.

 $<sup>^8</sup>$  Using the maximum possible TOV mass  $M=2.01\,M_\odot$  (instead of the maximum TOV mass in the third family  $M=2.00\,M_\odot$ ) to normalize mass scales for EOS A6 has negligible impact on our results.

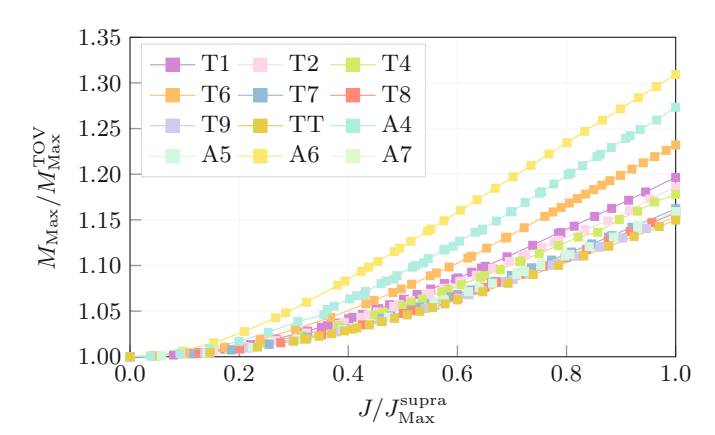


**Fig. 5.** Maximum mass along J-constant sequences of uniformly rotating equilibrium models as a function of the angular momentum J normalized to  $J_{\rm Max}^{\rm supra}$  (the angular momentum of the most massive star on the mass-shedding sequence). There is a non-negligible dependence on the EOS, and the supramassive limit for EOSs in table 1 varies from  $1.15\,M_{\rm Max}^{\rm TOV}$  (for EOS TT) to  $1.31\,M_{\rm Max}^{\rm TOV}$  (for EOS A6). Given this result, the constraints put on the EOS that employed the universality of the supramassive limit are valid only in the context of hadronic EOSs.

was combined with the observation of gravitational waves from event GW170817 to set an upper bound on the TOV limit mass. We repeat here the same argument to highlight the differences when EOSs with a hadron-quark phase transition are considered.

As shown by simulations, the observed properties of the gamma-ray burst and the ejecta following GW170817 suggest that the event left a rotating remnant supported by differential rotation. The remnant subsequently underwent delayed collapsed to a black hole (as argued out in [16] where the estimated ejecta mass was considered, see also [20, 25]), meaning that its mass was above the supramassive limit  $M_{\rm Max}^{\rm supra}$ . As we already mentioned, for hadronic EOSs it is possible to write

$$M_{\mathrm{Max}}^{\mathrm{supra}} = \alpha M_{\mathrm{Max}}^{\mathrm{TOV}},$$
 (12)

with  $\alpha \approx 1.2$ , independently of the EOS. Then, assuming the low-spin prior LIGO analysis for GW170817, the total gravitational mass of the system as inferred by the gravitational wave signal is  $M_{\rm tot} \approx 2.74^{+0.04}_{-0.01} \, M_{\odot}$  [10], and since this quantity has to be greater than the supramassive limit, the following holds

$$M_{\rm tot} \approx 2.74\,M_{\odot} > M_{\rm Max}^{\rm supra} = \alpha M_{\rm Max}^{\rm TOV}.$$
 (13)

With this inequality, the authors of [20,25] placed a constraint on the value of the maximum mass of a non-rotating configuration

$$M_{\rm Max}^{\rm TOV} < \frac{M_{\rm tot}}{\alpha} \approx 2.28 \, M_{\odot}.$$
 (14)

Figure 5 shows the loss of EOS-independence of the supramassive limit mass, which can be between 15% to 31% more than the TOV limit mass. Assuming that we

**Table 2.** Supramassive limit  $M_{\rm Max}^{\rm supra}$  and maximum mass for uniformly rotating stars belonging to the third family  $M_{\rm Max,third}^{\rm supra}$  for the EOSs considered in this paper (table 1). With the exception of T6, A4 and A6, for all the EOSs the most massive star belongs to the third family. For the other three EOSs, the maximum mass occurs in the phase transition (see fig. 4).

EOS	$M_{ m Max}^{ m supra}$	$M_{ m Max}^{ m supra}$	$M_{ m Max,third}^{ m supra}$	$M_{ m Max,third}^{ m supra}$		
	$[M_{\odot}]$	$M_{ m Max}^{ m TOV}$	$[M_{\odot}]$	$M_{ m Max}^{ m TOV}$		
T1	2.39	1.20	2.39	1.20		
T2	2.37	1.19	2.37	1.19		
T4	2.36	1.18	2.36	1.18		
T6	2.46	1.23	2.34	1.17		
T7	2.32	1.16	2.32	1.16		
T8	2.31	1.16	2.31	1.16		
T9	2.31	1.15	2.31	1.15		
TT	2.32	1.15	2.32	1.15		
A4	2.56	1.27	2.34	1.17		
A5	2.30	1.15	2.30	1.15		
A6	2.63	1.31	2.33	1.16		
A7	2.32	1.16	2.32	1.16		

can extend eq. (12) to include hybrid stars with 1.15  $\leq \alpha \leq$  1.31, using the same steps as in the case of hadronic EOSs the upper bound when hybrid EOSs are considered is revised to

$$2.07 M_{\odot} \lesssim M_{\text{Max}}^{\text{TOV}} \lesssim 2.38 M_{\odot}.$$
 (15)

The lower bound in eq. (15) comes from most recent massive pulsar J0740+6620 [114]. The upper bound is relaxed from  $2.28\,M_\odot$  to  $2.38\,M_\odot$  to encompass the EOSs treated in this work.

The assumption that we can extend eq. (12) (with  $1.15 \le \alpha \le 1.31$ ) to include hybrid stars, should be further tested using hybrid hadron-quark EOS with different baseline hadronic EOSs. But, this goes beyond the scope of the current work. However, that GW170817 is compatible with hybrid EOSs based on the fact that the supramassive limit mass should be smaller than the inferred mass from GW170817 is demonstrated in table 2, where we show the supramassive limit mass and the supramassive limit in the third family with each of the EOSs we treat in this work. As is evident from the table, the largest supramassive limit corresponds to EOS A6 which is  $2.63\,M_\odot$ , and hence safely smaller than even  $2.73\,M_{\odot}$  (the lower limit on the mass from GW170817). This result lends further support to the finding of [47] that GW170817 can be interpreted as the inspiral of a binary hybrid star-neutron star.

#### 4.2 Universal relations for turning points

Turning points mark the onset of a radial instability of the star, and provide a sufficient condition for secular axisymmetric instability in uniformly rotating (isentropic) stars [91, 92, 94, 117] (see also [118, 119]). Top turning points identify an instability to collapse and in the case of our EOSs designate the most massive hybrid stars. On the other hand, the bottom turning points single out the least massive twin stars. For this reason, universal relations involving turning point models are useful when studying the stability of rotating stars. In this section, we focus on the turning points in the third family of compact objects and discover a new relation, similar to eq. (11), for both top and bottom turning points. We also test the universal relations reported in [90], where it was shown that the angular momentum and masses of differentially rotating turningpoint models satisfy relations that are approximately independent of either the degree of differential rotation (and hence apply to uniformly rotating stars) or the EOS.

#### 4.2.1 Top turning points

To normalize the top turning point mass and angular momentum we first define the "Kepler turning point" configuration in the  $(\epsilon_c, M)$  plane as the model that lies at the intersection of the mass-shedding sequence with the turning-point line, i.e., the line connecting the top turning points along J-constant sequences. Note that the Kepler turning point model is neither the most massive nor more massive than the supramassive limit in the third family (see, e.g., fig. 4), but is very close to the supramassive limit of the third family. The same behavior was found for hadronic equations of state in [120]. To study universal relations of top turning points, we normalize their angular momentum with that of the Kepler turning point, which we denote  $J_{\text{Kep}}$ . In practice, we find the Kepler turning point by least-squares fitting the turning-point line with a fifth-order polynomial, and extending the resulting function until it intersects the mass-shedding sequence. Given that for each EOS we construct between 15 and 40 Jconstant sequences, we never need to extrapolate more than 1% out of the range of energy densities where we have data.

In fig. 6 we plot the top turning point mass normalized by the TOV limit mass *versus* the top turning point normalized angular momentum. The plot displays a stronger degree of universality compared to the one for the most massive models (fig. 5). The best-fitting function is

$$\frac{M_{\uparrow}}{M_{\rm Max}^{\rm TOV}} = 1 + 0.215 \left(\frac{J}{J_{\rm Kep}}\right)^2 - 0.050 \left(\frac{J}{J_{\rm Kep}}\right)^4. \quad (16)$$

This expression approximates all the EOSs we study here with a spread of at most 3%, which is only a little larger than the 2% spread found for hadronic EOSs [66]. As in the case of [66], the spread increases with the angular momentum, and for  $J/J_{\rm Kep} \lesssim 0.5$  all the EOSs agree with eq. (16) to within approximately 1%. The spread at higher angular momenta is mostly due to EOSs T1, T2 and T4.

By use of eq. (16), we can also find the supramassive limit mass of the third family  $M_{\rm Max,third}^{\rm supra}$ . This is because

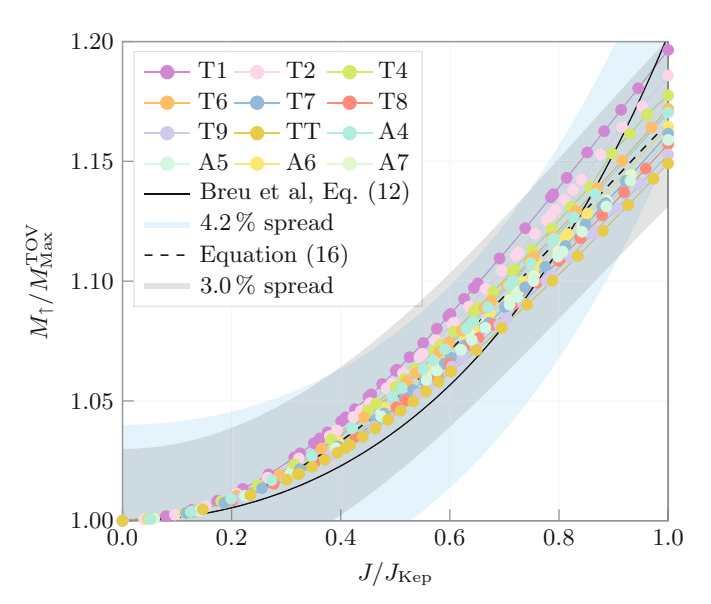


Fig. 6. Normalized gravitational mass of the top turning point on J-constant sequences of uniformly rotating equilibrium models of stars in the third family vs. the configuration's normalized angular momentum J. The gray shaded region is the 3% spread. Note that in [66]  $j/j_{\rm Kep}$  is used instead of  $J/J_{\rm Kep}$ , where  $j=J/M_{\rm Max}^2$  and  $j_{\rm Kep}=J_{\rm Kep}/M_{\rm Max}^2$ . The two quantities are the same, only the notation is different. For the EOSs in the Set I (see sect. 2) there is a correlation between  $M_{\uparrow}/M_{\rm Max}^{\rm TOV}$  and the value of jump  $\xi$ : for fixed  $J/J_{\rm Kep}$ , the smaller  $\xi$  is, the larger  $M_{\uparrow}/M_{\rm Max}^{\rm TOV}$  is. This can be clearly seen for EOSs T1, T2, and T4 (the first three curves from top to bottom).

the flatness of the mass-shedding sequence near the supramassive limit (see for example figs. 3 and 4) ensures that the Kepler turning point mass agrees with the supramassive limit mass of the third family to better than 0.1% for all EOSs we consider. Moreover, the error in estimating the supramassive limit mass due to considering the Kepler turning point angular momentum instead of the supramassive limit angular momentum is smaller than the dependence from the EOS. Plugging  $J=J_{\rm Kep}$  in eq. (16), we obtain

$$M_{\rm Max,third}^{\rm supra} = (1.165 \pm 0.035) M_{\rm Max}^{\rm TOV},$$
 (17)

where the spread corresponds to the largest discrepancy from the mean value in the set of EOSs we study (shown as the gray shaded region in fig. 6).

In fig. 6 we also compare our finding with the universal relation of [66], since turning points were considered there, too. We find that if we allow for a 3% spread, eq. (12) in [66] holds up to  $J/J_{\rm Kep} \approx 0.85$ , but overestimates the mass for larger angular momenta. Equation (12) of [66] can describe the EOSs studied here with larger angular momenta with an increased spread of 4.2% (cyan shaded region in fig. 6). Thus, our expression (16) provides a better fit to the data, and as is clear from fig. 6, eq. (16) better captures the trend of the data.

Finally, we note that for the EOSs of Set I, there is a correlation between the jump size  $\xi$  and the value

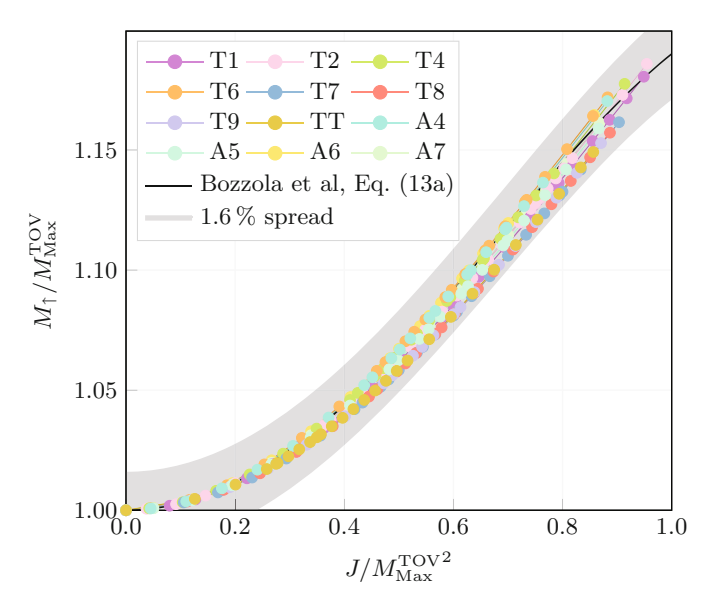


Fig. 7. EOS-independent relation between angular momentum and gravitational mass of the top turning points for *J*-constant sequences of uniformly rotating stars. The solid line is eq. (13a) in [90], with a 1.6% spread indicated by the shaded region. This relation is satisfied by all the EOSs of table 1. Moreover, the relation provides a different parametrization of eq. (16) with smaller spread.

of  $M_{\uparrow}$ : for a given value of  $J/J_{\rm Kep}$ ,  $M_{\uparrow}/M_{\rm max}^{\rm TOV}$  is larger for EOSs with smaller  $\xi$  (as is clear from the top three curves in fig. 6). As a result, T1 has the largest normalized maximum mass  $(1.19\,M_{\rm Max}^{\rm TOV})$  and TT the smallest  $(1.15\,M_{\rm Max}^{\rm TOV})$ . This does not happen for the EOSs in Set II which are all comparable (regardless of the width of the phase transition) and have no emerging trend.

Next, we consider the EOS-independent relations found in [90] between angular momentum, gravitational and rest mass of top turning points, which we report here for convenience

$$\begin{split} \frac{M_{\uparrow}}{M_{\rm Max}^{\rm TOV}} &= 1 + 0.29 \left(\frac{J}{M_{\rm Max}^{\rm TOV^2}}\right)^2 - 0.10 \left(\frac{J}{M_{\rm Max}^{\rm TOV^2}}\right)^4, \\ \frac{M_{0,\uparrow}}{M_{0,\rm Max}^{\rm TOV}} &= 1 + 0.51 \left(\frac{J}{M_{0,\rm Max}^{\rm TOV^2}}\right)^2 - 0.28 \left(\frac{J}{M_{0,\rm Max}^{\rm TOV^2}}\right)^4, \end{split} \tag{18a}$$

$$\frac{M_{0,\uparrow}}{M_{0,\text{Max}}^{\text{TOV}}} = 0.93 \frac{M_{\uparrow}}{M_{\text{Max}}^{\text{TOV}}} - 0.07. \tag{18c}$$

Figure 7 depicts these quantities and shows that the top turning points are aligned with the previously known equation. In fact, we find that these models satisfy all the three relations (18) with the same spread as hadronic EOSs (1.6% for eq. (18a)<sup>9</sup> and 1.2% for eqs. (18b) and (18c)). This is a non-trivial result because in [90] it

was noted that purely quark stars described with the MIT bag model do not follow the same universal relations, even in the uniform rotation case. Nonetheless, here we find that for the EOSs of Set I, which employs a variant of the MIT bag model for the high-density phase, the relations are still satisfied. This suggests that the hadronic low-density part plays an important role in determining the universality.

#### 4.2.2 Bottom turning points

We discovered that bottom turning points satisfy a relation similar to eq. (16), if the normalizing angular momentum is that of the Kepler bottom turning point (found at the intersection of the bottom turning-point line with the mass shedding sequence)

$$\frac{M_{\downarrow}}{M_{\perp}^{\text{TOV}}} = 1 + 0.33 \left(\frac{J}{J_{\downarrow,\text{Kep}}}\right)^2 - 0.10 \left(\frac{J}{J_{\downarrow,\text{Kep}}}\right)^4. \quad (19)$$

The spread in this equation is at most  $2\%^{10}$ .

Moreover, we find that the bottom turning points can be described with the same eqs. (18), but with a spread of 3%. The universality becomes tighter if we consider top and bottom turning points separately. For the bottom turning points, the best-fitting functions are

$$\begin{split} \frac{M_{\downarrow}}{M_{\downarrow}^{\text{TOV}}} &= 1 + 0.35 \left(\frac{J}{M_{\downarrow}^{\text{TOV}^2}}\right)^2 - 0.12 \left(\frac{J}{M_{\downarrow}^{\text{TOV}^2}}\right)^4, \\ \frac{M_{0,\downarrow}}{M_{0,\downarrow}^{\text{TOV}}} &= 1 + 0.58 \left(\frac{J}{M_{0,\downarrow}^{\text{TOV}^2}}\right)^2 - 0.35 \left(\frac{J}{M_{0,\downarrow}^{\text{TOV}^2}}\right)^4, \\ \frac{M_{0,\downarrow}}{M_{0,\downarrow}^{\text{TOV}}} &= 1.016 \frac{M_{\downarrow}}{M_{\downarrow}^{\text{TOV}}} - 0.016, \end{split} \tag{20b}$$

with largest spread of 1% for the first two and 0.2% for the last. Figure 8 shows eq. (20a), and in the inset we compare it to eq. (18a), which is the corresponding universal relation for top turning points. Among the three universal relations, eqs. (20a) and (18a) are the ones in which top and bottom turning point differ the most.

#### 5 Differential rotation

In this section we consider differentially rotating stars with hybrid EOSs and compute the maximum mass that can be supported. In this context, it is more common to consider the rest mass instead of the gravitational mass [65]. Nevertheless, the results that will follow are qualitatively the same also for the gravitational mass.

<sup>&</sup>lt;sup>9</sup> This relation carries similar information compared to eq. (16), and exhibits better universality.

Note that T1, T2, T4 do not have any bottom turning point.

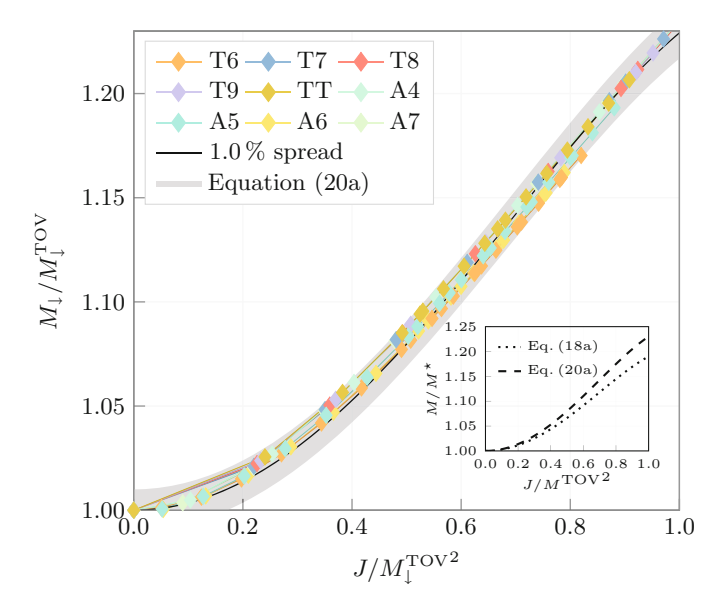


Fig. 8. Same as fig. 7, but for bottom turning points. Here the solid line is eq. (20a), and the shaded region is the 1% spread. Bottom turning points satisfy an EOS-independent relation. In the inset we compare the universal relations for top and bottom turning points, eqs. (18a) and (20a).

The KEH rotation law of eq. (6) produces stars with two different topologies: spheroidal and quasi-toroidal. In quasi-toroidal configurations the maximum energy density occurs in a ring around the stellar geometric center, whereas in spheroidal stars the location of the maximum energy density coincides with geometric center of the star. Examples of such configurations are reported in fig. 9, where we show meridional energy density contours for a spheroidal and a quasi-toroidal solution. In this paper, we focus primarily on spheroidal models because quasi-toroidal configurations are likely to be unstable [80].

#### 5.1 Maximum mass

To find the maximum rest mass for each EOS, we fix the degree of differential rotation  $\hat{A}^{-1}$ , and scan the maximum energy density in the range  $\epsilon_{\rm max} \in (0.5,3)\,10^{15}\,{\rm g\,cm^{-3}}$ , which is where the most massive models always lie for the EOSs considered here. For each value of  $\epsilon_{\rm max}$  we construct equilibrium models with decreasing value of  $r_p/r_e$  until we find a quasi-toroidal solution or we reach the mass-shedding limit. The last configuration built before the quasi-toroidal or mass-shedding limit is reached is the maximum mass for that value of  $\epsilon_{\rm max}$  in our search.

In fig. 10 we show the maximum rest mass normalized to the rest-mass of the TOV limit as a function of  $\hat{A}^{-1}$ . The behavior is similar to that seen for polytropes [76] and hadronic EOSs [72] and it is followed very closely by the gravitational mass: at relatively low values of  $\hat{A}^{-1}$  ( $\lesssim 0.25$ ), corresponding to rotational profiles closer to uniform rotation, there are only modest increases in the rest mass, not exceeding 40%. For higher values of  $\hat{A}^{-1}$ , the increase of  $M_{0,\text{Max}}$  compared to the TOV limit grows until it

reaches a maximum and then begins to decrease again as  $\hat{A}^{-1}$  is increased further. The largest gain in rest mass is seen for EOS A6 (123% more than the TOV limit), which is also the EOS with the highest gain in the supramassive limit (see sect. 4).

In table 3 we report relevant properties of the most massive spheroidal models found in our search of the parameter space. Larger increases in the rest mass are possible if we consider quasi-toroidal stars and possibly other differential rotation laws. Thus, these masses should be considered as lower-limits on the maximum mass of even spheroidal stars. Moreover, finding the "absolute" maximum rest mass model for hybrid EOSs with the KEH law depends sensitively on the resolution in  $\epsilon_{\rm max}$ ,  $r_p/r_e$ , and  $\hat{A}^{-1}$  used to scan the parameter space. For the models presented in table 3 we use a step in  $\epsilon_{\text{max}}$  and  $r_p/r_e$  of 0.01, and a step in  $\hat{A}^{-1}$  of 0.005. Even with this high resolution in  $\hat{A}^{-1}$ , we found large increases in the rest mass over small ranges of  $\hat{A}^{-1}$ . Such increases in mass correspond to a transition to a different solution type, as shown in the inset of fig. 10, where we show the maximum rest mass type A models along with the maximum rest mass spheroidal solutions (which also include type C models) for the A4 EOS. We explore the maximum rest mass of each solution type in appendix A, where more details on the different types of solutions of differentially rotating stars are also presented.

#### 5.2 Universal relations

In [90] it was found that for hadronic EOSs and restricting to spheroidal models, eq. (18) applies not only to uniformly rotating stars, but also to differentially rotating stars, and, what is more, the relation is approximately insensitive to the degree of differential rotation (with maximum spread of about 1% even for high degrees of differential rotation). Moreover, recently, in [78] it was noted that for purely strange quark-matter stars the relations between angular momentum and masses of turning points follow equations approximately independent of  $\hat{A}^{-1}$  (with spread below 2%), although the relation is not the same as for hadronic EOSs [90]. Here, we construct sequences of differentially rotating equilibrium models with constant angular momentum and various degrees of differential rotation in the range  $\hat{A}^{-1} \in (0,2)$  to test whether this property holds for the hybrid hadron-quark EOSs we treat in this work.

We find that relations (18) apply approximately to hybrid EOSs for degrees of differential rotation  $\hat{A}^{-1} \in (0, 2)$ , but with a larger spread of about 3% and with an evident (albeit weak) dependence on  $\hat{A}^{-1}$ . Furthermore, the larger the degree of differential rotation, the larger the spread becomes. For this reason, the universality found in [90] appears to be broken in the case of hybrid stars.

For top turning points, we show an example of the above conclusions in fig. 11, where we report the results from J-constant sequences constructed with EOS TT. We found that there is a correlation between the jump size

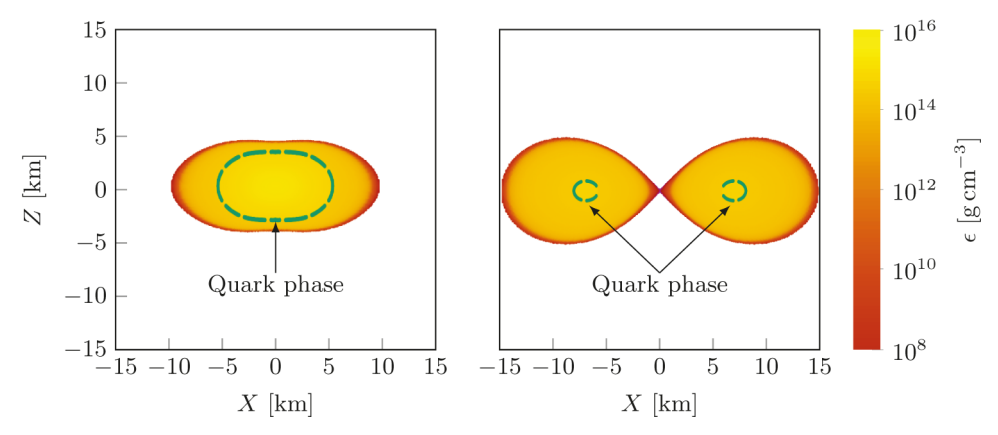


Fig. 9. Examples of meridional contours of the energy density for spheroidal (left) and quasi-toroidal (right) stars for EOS A5. The green dashed line locates the quark core by outlining the contour where the energy density equals the value of energy density at the onset of the phase transition.

Table 3. Maximum rest mass spheroidal models for the EOSs considered in this work. Shown are the values of the degree of differential rotation  $\hat{A}^{-1}$ , the maximum energy density  $\epsilon_{\rm max}$  in units of  $10^{15}\,{\rm g\,cm^{-3}}$ , the ratio of polar to equatorial radius  $r_p/r_e$ , the ratio of kinetic to gravitational potential energy T/|W|, the ratio of central to equatorial angular velocity  $\Omega_c/\Omega_e$ , the circumferential radius at the equator  $R_e$  in units of km, the dimensionless spin  $J/M^2$ , the mass  $M_{\rm ADM}$  in units of  $M_{\odot}$ , the ratio of the mass  $M_{\rm ADM}$  to the TOV limit mass  $M_{\rm Max}^{\rm TOV}$ , the rest mass  $M_0$  in units of  $M_{\odot}$  and the ratio of the rest mass to TOV limit rest mass  $M_{0,{\rm Max}}^{\rm TOV}$ . The increase in maximum mass compared to the non-rotating limit is between  $\sim 40\%$  and  $\sim 123\%$ . Quantities of particular interest are T/|W| that can be larger than  $\sim 0.26$ , which is the threshold for the dynamical bar mode instability (see e.g. [62] for a review), and the rest mass which can be larger than twice the TOV limit – such configurations are classified as ubermassive according to [72].

EOS	$\hat{A}^{-1}$	$\epsilon_{ m max}$	$r_p$	$\underline{T}$	$\underline{\Omega_c}$	$R_e$	$\underline{J}$	M	$\underline{M}$	$M_0$	$M_0$
		$[10^{15}\mathrm{gcm^{-3}}]$	$r_e$	W	$\Omega_e$	$[\mathrm{km}]$	$M^2$	$[M_{\odot}]$	$M_{ m Max}^{ m TOV}$	$[M_{\odot}]$	$M_{0,\mathrm{Max}}^{\mathrm{TOV}}$
T1	0.390	1.03	0.35	0.265	1.930	18.25	0.922	3.860	1.563	4.526	1.542
T2	0.410	1.09	0.32	0.276	1.965	19.35	0.943	3.974	1.720	4.662	1.699
T4	0.415	1.23	0.31	0.280	1.990	19.53	0.948	4.008	1.847	4.699	1.842
Т6	0.425	1.38	0.30	0.283	2.038	19.58	0.952	4.018	2.004	4.705	1.971
T7	0.415	1.71	0.36	0.247	2.064	14.70	0.892	3.097	1.447	3.633	1.393
Т8	0.395	2.07	0.38	0.238	2.040	13.55	0.878	2.944	1.415	3.450	1.368
Т9	0.420	2.08	0.38	0.235	2.079	13.49	0.875	2.845	1.408	3.325	1.361
TT	0.430	2.22	0.38	0.234	2.116	13.11	0.872	2.758	1.393	3.216	1.356
A4	0.405	1.11	0.26	0.304	1.985	22.69	0.985	4.688	2.222	5.593	2.275
A5	0.510	0.89	0.28	0.293	1.990	23.07	1.013	3.951	1.976	4.577	1.937
A6	0.410	1.31	0.25	0.305	2.036	22.00	0.983	4.557	2.279	5.431	2.334
A7	0.490	0.96	0.28	0.292	1.992	22.44	1.000	4.013	2.007	4.675	1.987

 $\xi$  and the loss of the universality: the larger the jump, the stronger the deviation from universality. Hence, the example in fig. 11 is one of the cases that violates the universality the strongest. For most of the EOSs we treat, the bottom turning point universal relations exhibit a smaller spread with increasing  $\hat{A}^{-1}$  (below 2%), but they still violate eqs. (20) for some EOSs, as reported in fig. 12 for EOS A7. For this EOS, the deviation from eqs. (20) can be up to 4%.

Both fig. 11 and 12 show that there is a clear dependence on  $\hat{A}^{-1}$ . Hence, we conclude that the universal relations found in [90] are EOS-independent for uniform ro-

tation, but not for differential rotation, as they acquire a dependence on  $\hat{A}^{-1}$  which is not the same for all the EOSs. The regularity and smoothness of sequences in the figures suggests that it is possible to parametrize the dependence on  $\hat{A}^{-1}$  using some scale characteristic of the EOS. However, exploring this goes beyond the scope of the current work.

Finally, we point out that for sufficiently high values of  $\hat{A}^{-1}$  and J, in some EOSs the J-constant sequences exhibit no bottom turning points. This is because stars whose central energy density is in the phase transition region become more massive when spun up compared to the

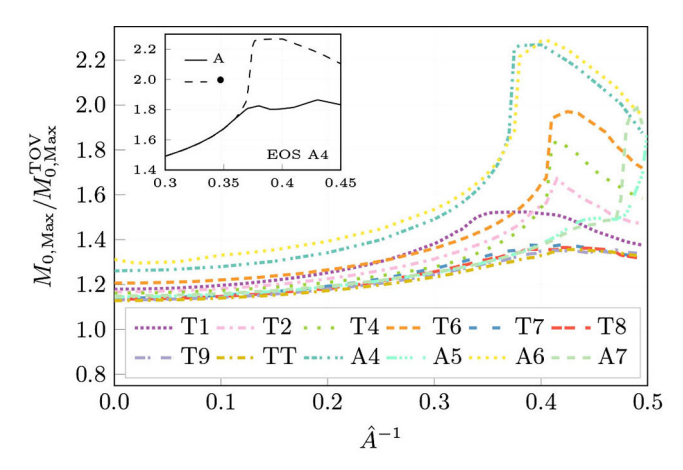


**Fig. 10.** Maximum rest mass normalized to the TOV limit rest mass  $M_{0,\mathrm{Max}}/M_{0,\mathrm{Max}}^{\mathrm{TOV}}$  as a function of degree of differential rotation  $\hat{A}^{-1}$  for each EOS in our study (table 1). We only show the curves relevant for the maximum rest mass of spheroidal stars. In the inset we show the increase in mass for EOS A4 including all spheroidal stars and only type A stars (see appendix A).

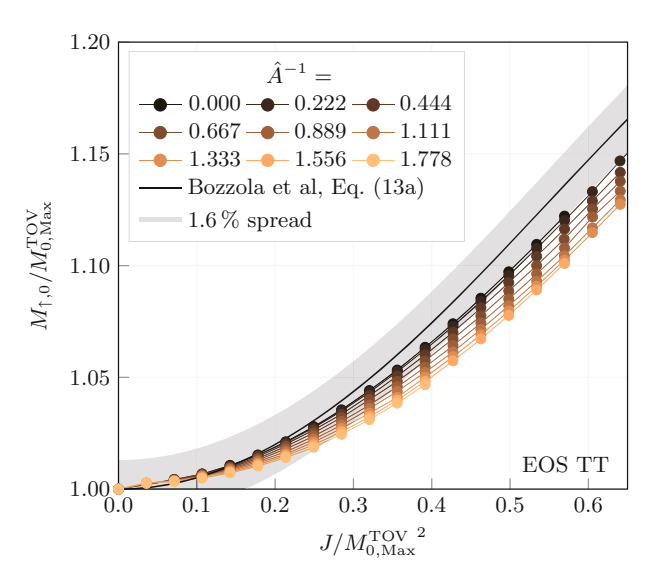


Fig. 11. Normalized rest mass as a function of the normalized angular momentum for top turning points on J-constant sequences with various degrees of differential rotation. The plot corresponds to EOS TT. The turning points are compatible with the previously known relation only in the case of uniform rotation, but there is a clear dependence on the degree of differential rotation. This is the case where the violation of the universal relation satisfied by the uniformly rotating case is the most evident, and shows that the relations found in [90] cannot be considered  $\hat{A}^{-1}$ -independent for the EOSs considered in this work.

ones with higher central energy density. This means that J-constant sequences in the  $(\epsilon_c, M)$  plane tend to become flatter and have shallower dips (see, for example, fig. 4). In some other cases with high degree of differential rotation and angular momentum we could not even identify the top turning point, because the change of concavity is not resolved by the accuracy of our code.

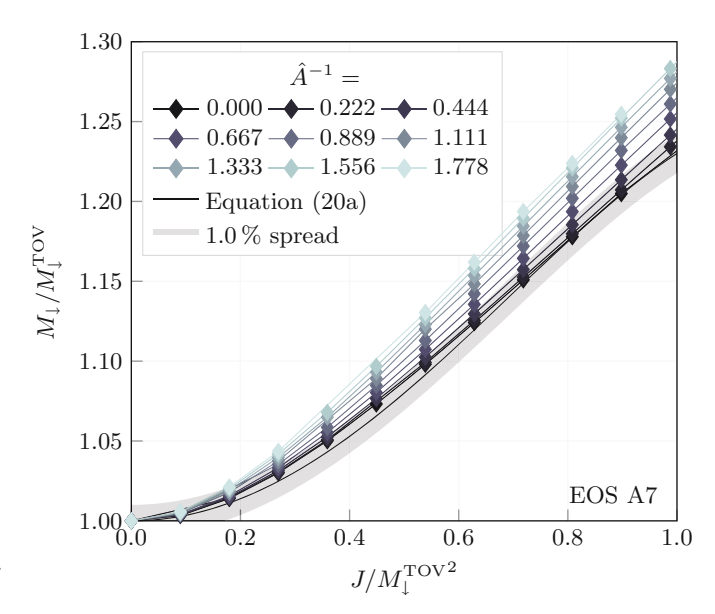


Fig. 12. Similar to fig. 11, but for rest mass and angular momentum of bottom turning points, and for EOS A7. In this case, too, there is a clear dependence on the degree of differential rotation, and so eqs. (20) are not  $\hat{A}^{-1}$ -independent. Among the EOS considered in this study, this is the EOS with the strongest violation of the universal behavior.

#### 6 Conclusions

The equation of state of nuclear matter is uncertain at densities larger than nuclear saturation density  $\rho_0$ . Some of the proposed EOS models undergo a phase transition from hadronic to quark matter which can result in hadron-quark hybrid stars. For EOSs with a sufficiently large jump in energy density over which the pressure remains constant, a third family of compact objects emerges. In this work we analyzed the properties of rotating relativistic stars using EOSs with first-order hadron-quark phase transitions for many of which a third family of stars emerges. To be more specific, we employed the quark matter parametrizations introduced in [47] for the EOSs developed in [29] and [46].

We employed the Cook code [60, 63] to build rotating relativistic stars and we studied equilibrium sequences with constant angular momentum and varying central energy density. We found that the maximum mass a uniformly rotating hybrid star can support (the so-called supramassive limit) is not an EOS-independent quantity, but it varies from 15% to 31% more than the TOV limit mass, in contrast to previous work [64, 66] which highlighted an approximately EOS-independent increase of about 20% for hadronic EOSs. This implies that some constraints placed on the equation of state based on the universality of the supramassive limit and GW170817 [20,25] do not apply to EOSs like the ones considered here. However, the supramassive limit mass of the EOSs we adopt is consistent with GW170817, providing further support that hybrid hadron-quark EOSs can describe GW170817.

We located the turning points on constant angular momentum sequences, which are identified by the stationarity condition of eq. (10). We defined the bottom and top turning points along a J-constant sequence as those that correspond to the least massive twin star and the most massive star in the third family, respectively. Top turning points satisfy a universal relation (eq. (16)) with spread of about 3%. With this relation, we found that the supramassive limit of the third family is given by

$$M_{\rm Max,third}^{\rm supra} = (1.165 \pm 0.035) M_{\rm Max}^{\rm TOV}.$$
 (21)

Enabling differential rotation and focusing on spheroidal models, we found that the maximum mass (both baryonic and gravitational) can increase by as much as 123% compared to the non-rotating case. This enhancement compared to the TOV limit mass, represents a lower limit of what can be achieved with differential rotation.

Finally, we investigated the applicability of universal relations for turning points found in [90], who reported relations between the angular momentum, and the masses of turning points that are independent of the EOS and the degree of differential rotation. We found that the relations in [90] hold for the top turning points for uniformly rotating stars. We also discovered similar universal relations for the bottom turning points for uniformly rotating stars. However, both universal relations are violated when differential rotation is enabled.

In future work we will consider constant rest-mass sequences, and explore additional hybrid equations of state with varying baseline hadronic EOSs, to further test some of the results we reported in this work.

We are grateful to S. L. Shapiro for access to the code that we used to build equilibrium models for rotating relativistic stars, and to D. Alvarez-Castillo, D. Blanschke and A. Sedrakian for giving us permission to use the equations of state developed in [47]. We also thank N. Stergioulas for access to the RNS code [120, 121] that was used to cross-check some of the results presented here. This work has been supported in part by National Science Foundation Grant Number PHY-1912619 at The University of Arizona. Computations were in part performed on the Ocelote cluster at The University of Arizona. This research used also resources provided by the Open Science Grid [122], which is supported by the National Science Foundation and the U.S. Department of Energy's Office of Science.

**Data Availability Statement** This manuscript has no associated data or the data will not be deposited. [Authors' comment: All data generated during this study are contained in this published article.]

**Publisher's Note** The EPJ Publishers remain neutral with regard to jurisdictional claims in published maps and institutional affiliations.

# Appendix A. Solution space of differentially rotating stars

In this appendix we discuss the solution space of equilibrium models for stars rotating with the KEH law of eq. (6). We find features in the solution space which are consistent with both hadronic and strange quark star EOSs, while also finding others which are unique to hybrid EOSs. In the case of differential rotation with the KEH law, solutions for a given maximum energy density can be separated on the  $(r_p/r_e, \hat{\beta})$  plane into four classes depending on the degree of differential rotation. These classes are known as types A, B, C and D [75]. The first, type A, consists of spheroidal configurations with a relatively low degree of differential rotation. All uniformly rotating stars, if seen as differentially rotating with  $\hat{A}^{-1} = 0$ , belong to this family. Type B solutions are characterized by a high central angular velocity but relatively low degree of differential rotation. These models are quasi-toroidal, since the maximum energy density does not occur in the geometric center of the star. In fig. 9, we show a comparison between the energy density profiles of a type A and a type B solution. The third category (type C) contains spheroids and quasi-toroids with higher degrees of differential rotation than types A and B. Finally, type D stars are typically highly pinched at the equator and quasi-toroidal. We were unable to construct type D solutions with the Cook code, but this is not a severe limitation on our study since these configurations are not likely to be found in Nature because their sequences start from a mass-shedding limit and end at a mass-shedding limit [76].

The classification of different solution types works as follows: for a fixed value of  $\epsilon_{\text{max}}$ , there exists a critical value of the degree of differential rotational  $\hat{A}_{\text{crit}}^{-1}$ , defined by the condition

$$\left. \frac{\partial \hat{A}^{-1}}{\partial (r_p/r_e)} \right|_{\epsilon_{\text{max}}} = 0 = \left. \frac{\partial \hat{A}^{-1}}{\partial \hat{\beta}} \right|_{\epsilon_{\text{max}}}.$$
 (A.1)

The function  $\hat{\beta}(r_p/r_e)$  that corresponds to  $\hat{A}_{\rm crit}^{-1}$  for a given energy density is referred to as the "separatrix". This quantity partitions the solution space into four regions, each corresponding to a different solution type. Models are classified directly using the separatrix in the  $(r_p/r_e, \hat{\beta})$  plane, as shown in fig. 13, where we show the separatrix for EOS A5 at energy density  $0.5 \times 10^{15} \, {\rm g \ cm^{-3}}$ . Figure 13 is consistent with the results observed for polytropic and hadronic EOSs [72, 75]. However, since we were not able to build type D stars, there are three regions instead of four in fig. 13.

In practice, instead of working directly with the separatrix, it is more convenient to consider  $\hat{A}_{\rm crit}^{-1}$  as a function of maximum energy density in order to assign a type to a configuration. For a fixed EOS and  $\epsilon_{\rm max}$ , all equilibrium models with  $\hat{A}^{-1} < \hat{A}_{\rm crit}^{-1}$  are of either type A or B, whereas those with  $\hat{A}^{-1} > \hat{A}_{\rm crit}^{-1}$  are of type C (or D). Then, a solution is categorized as spheroidal if the maximum energy density occurs in the center of mass. Since we do not

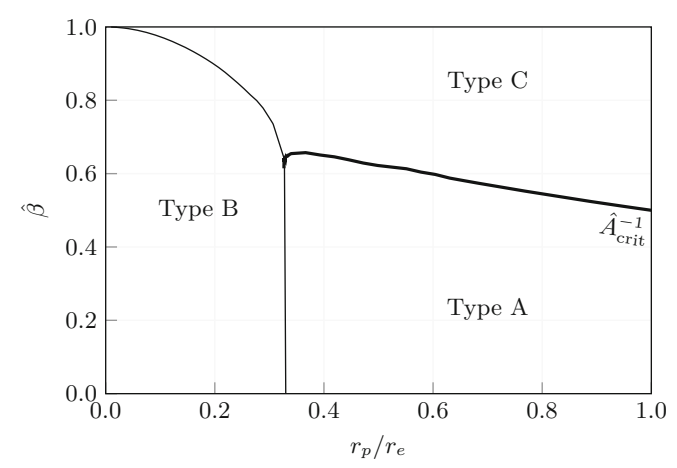


Fig. 13. Mass-shedding parameter  $\hat{\beta}$ , calculated using eq. (9), as a function of the ratio of polar to equatorial radii  $r_p/r_e$  for a fixed energy density of  $\epsilon_{\rm max}=1.2\times 10^{15}~{\rm g~cm}^{-3}$ . The bold black line corresponds to the critical degree of differential rotation  $\hat{A}_{\rm crit}^{-1}=0.611$ , defined by the saddle point on the  $(r_p/r_e,\hat{\beta})$  plane at which all solution types we are able to construct with the Cook code co-exist for this value of the energy density (see fig. 2 in [75] for a complete plot for polytropes). The Cook code is not able to produce type D stars, which in this plot would reside at values of  $r_p/r_e \lesssim 0.33$  (the vertical leg of the separatrix), and  $0 \leq \hat{\beta} \lesssim 0.6$  [75].

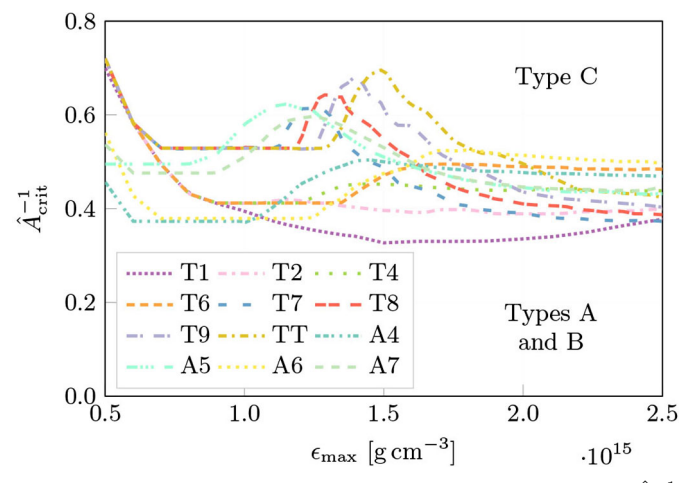


Fig. 14. Critical value of the degree of differential rotation  $\hat{A}^{-1}$  as a function of the maximum energy density  $\epsilon_{\rm max}$  for the EOSs in this study. Models of a given value of  $\epsilon_{\rm max}$  with  $\hat{A}^{-1} < \hat{A}_{\rm crit}^{-1}$  are type A or B models, and solutions with  $\hat{A}^{-1} > \hat{A}_{\rm crit}^{-1}$  are type C. For some values of  $\hat{A}^{-1}$ , equilibrium sequences with varying maximum energy density change the type along the sequence.

have control over  $\hat{\beta}$ , we cannot directly solve eq. (A.1) to find the critical value for  $\hat{A}^{-1}$ . Hence, as in [72], we estimate  $\hat{A}_{\rm crit}^{-1}$  with the maximum of the function  $\hat{A}_{\rm min}^{-1}(r_p/r_e)$ , where  $\hat{A}_{\rm min}^{-1}$  is the smallest degree of differential rotation for which an equilibrium model exists with the given maximum energy density. This method allows the calculation of  $\hat{A}_{\rm crit}^{-1}$  to within 1% accuracy [72].

Figure 14 shows the critical degree of differential rotation as a function of the maximum energy density for all the hybrid EOSs we consider in this work. The figure exhibits features which are unique to hybrid EOSs but which may be reconciled with the results of hadronic and strange-quark-matter EOSs. Crucially,  $\hat{A}_{\rm crit}^{-1}$  is not a monotonically decreasing function of  $\epsilon_{\rm max}$  (see footnote<sup>11</sup>) and, as a result, for some values of  $\hat{A}^{-1}$ , an equilibrium sequence with varying  $\epsilon_{\rm max}$  (such as the ones considered in sect. 5.2) can jump back and forth between being class A or B and C. The significant increases in mass that we find in sect. 5 correspond to a jump in models from type A to type C.

In [75], homogeneous stars described by an incompressible EOS in which

$$\epsilon(P) = \epsilon_0, \tag{A.2}$$

where  $\epsilon_0$  is a constant, were considered. For such an EOS, the pressure and energy density do not depend on one another, similar to the constant pressure regions of the EOSs studied in this work. In [75] it was found that the function  $\hat{A}_{\rm crit}^{-1}(\epsilon_{\rm max})$  for incompressible EOSs first increases to a maximum and subsequently decreases as the energy density increases. This same feature was observed for strange-quark-matter EOSs, which may be suitably approximated as homogeneous bodies [79]. We note that similar features appear in the curves presented in fig. 14 above the values of energy density corresponding to the constant pressure regions of the EOSs. It is possible that the "bump" features seen in the curves in fig. 14 arise for the same reasons as those found in [75] and [79] for homogeneous and strange-quark-matter EOSs, respectively.

In table 4 we list the maximum rest mass models found in our search for each solution type we were able to construct with the Cook code and for three representative EOSs. We focus on the T1, T8, and A6 EOSs to highlight particular features of the solution space. As can be seen from fig. 14, the "bump" feature of the function  $\hat{A}_{\text{crit}}^{-1}(\epsilon_{\text{max}})$  results in the appearance of A and B solutions at values of  $\epsilon_{\rm max}$  and  $\hat{A}^{-1}$  which are high compared to hadronic EOSs. Despite the presence of type A and B stars in larger regions of the parameter space compared to hadronic EOSs, we find that the maximum rest mass configurations still correspond to modest degrees of differential rotation and not for the largest energy densities considered. For all three EOSs, we find that the type B models are the most massive, which agrees with the findings from studies with hadronic EOSs [72]. The largest gain in mass is for EOS A6, with which it is possible to construct stars almost three times more massive than the corresponding TOV limit. This increase in rest mass is larger than the ones seen for the hadronic EOSs studied in [72]. Note that the type B stars tend to have the lowest value of  $\epsilon_{\rm max}$  among the maximum rest mass solutions, suggesting that these configurations predominantly sample from the low density part of the corresponding EOS.

 $<sup>^{11}</sup>$  We refer to the increase and subsequent decrease of  $\hat{A}_{\rm crit}^{-1}(\epsilon_{\rm max})$  at values of  $\epsilon_{\rm max}$  above the phase transition (as shown in fig. 14) as a "bump" feature.

Table 4. Maximum rest mass differentially rotating models for the T1, T8, and A6 EOSs. Shown are the solution types (A, B, or C), the value of the degree of differential rotation  $\hat{A}^{-1}$ , the maximum energy density  $\epsilon_{\text{max}}$  in units of  $10^{15} \, \text{g cm}^{-3}$ , the ratio of polar to equatorial radius  $r_p/r_e$ , the ratio of kinetic to gravitational potential energy T/|W|, the ratio of central to equatorial angular velocity  $\Omega_c/\Omega_e$ , the circumferential radius at the equator  $R_e$  in units of km, the dimensionless spin  $J/M^2$ , the ADM mass M in units of  $M_{\odot}$ , the ratio of the mass to the TOV limit mass, the rest mass in units of  $M_{\odot}$  and the ratio of the rest mass to TOV limit rest mass  $M_{0,\text{Max}}^{\text{TOV}}$ .

EOS	Type	$\hat{A}^{-1}$	$\epsilon_{ m max}$	$r_p$	$\underline{T}$	$\Omega_c$	$R_e$	$\underline{J}$	M	$\underline{M}$	$M_0$	$M_0$
			$[10^{15}\mathrm{gcm^{-3}}]$	$\overline{r_e}$	W	$\Omega_e$	[km]	$M^2$	$[M_{\odot}]$	$M_{ m Max}^{ m TOV}$	$[M_{\odot}]$	$M_{0,\mathrm{Max}}^{\mathrm{TOV}}$
T1	A	0.35	1.22	0.38	0.247	1.787	17.50	0.900	3.700	1.498	4.331	1.476
	В	0.35	0.56	0.01	0.332	1.756	27.18	1.047	5.764	2.333	6.744	2.299
	$^{\mathrm{C}}$	0.50	0.69	0.01	0.314	2.589	21.44	0.979	4.897	1.983	5.757	1.962
Т8	A	0.39	2.14	0.39	0.236	2.037	13.27	0.874	2.920	1.404	3.421	1.357
	В	0.35	0.56	0.01	0.332	1.756	27.18	1.047	5.764	2.771	6.744	2.675
	$^{\rm C}$	0.55	0.66	0.02	0.309	2.646	21.70	0.983	4.728	2.273	5.519	2.189
A6	A	0.37	1.21	0.38	0.243	1.584	20.97	0.923	3.638	1.819	4.281	1.840
	В	0.35	0.50	0.01	0.332	1.759	27.35	1.045	5.849	2.925	6.943	2.984
	$^{\rm C}$	0.45	0.58	0.01	0.318	2.380	22.99	0.987	5.327	2.664	6.392	2.748

Note also that for this reason the T1 and T8 type B models presented in table 4 are the same. The T1 and T8 EOSs are identical in the low density regime and begin to diverge at  $\epsilon \approx 0.66 \times 10^{15} \, \mathrm{g \, cm^{-3}}$ , whereas the maximum rest mass stars for each of these EOS have  $\epsilon_{\rm max} = 0.56 \times 10^{15} \, {\rm g \, cm^{-3}}$ . Because the maximum energy density of these configuration is the same, and, because the EOSs are identical below this energy density, the corresponding solutions are identical. Any EOS that is the same in the low density regime as the T1 EOS will have an identical maximum rest mass type B model (including T2, T4, T6, T7, T9, and TT). However, note that because of their different TOV masses, each of these EOSs exhibit a different maximal increase in the rest mass compared to the TOV limit rest-mass. The maximum rest mass type C solutions presented in table 4 are different between T1 and T8, because the corresponding values of  $\epsilon_{\rm max}$  are greater than the energy density at which the two EOS begin to diverge from one another. The models presented in table 4 are not the definitively most massive, but only the largest we were able to locate in the solution space. We were unable to scan the entire solution space using the Cook code (in particular we could not construct type D stars or highly pinched type B ones). Moreover, because different solution types can emerge as the maximum energy density changes, locating the absolute maximum rest mass models for the solution types we were able to compute depends on the resolution in the parameters  $\epsilon_{\text{max}}$ ,  $r_p/r_e$ ,  $\hat{A}^{-1}$  used to scan the solution space. We used a step in  $\epsilon_{\rm max}$  and  $r_p/r_e$  of 0.01 and a step in  $\hat{A}^{-1}$  of 0.01 for the class A, but a step of 0.05 for families B and C.

# Appendix B. Convergence in presence of a phase transition

In this appendix, we discuss the convergence properties of our numerical scheme. While the Cook code has been thor-

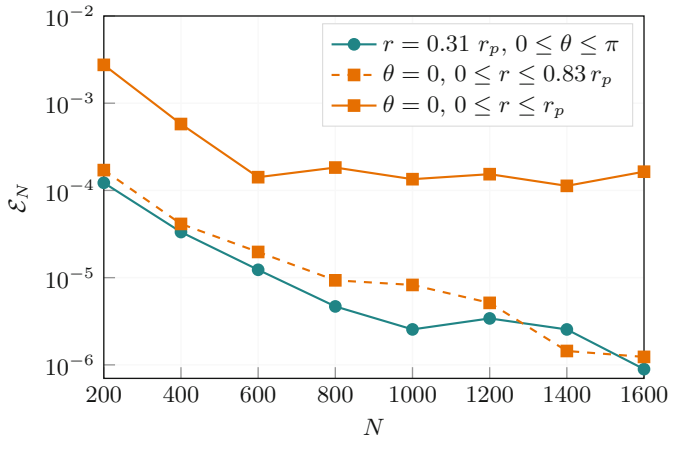


Fig. 15. Self convergence of the relative error in energy density  $\mathcal{E}_N$  (see eq. (B.1)) as a function of grid resolution at fixed angle (orange solid lines with square points) and fixed radius (teal solid line with round points). The grid resolution is N in the radial direction, and N/2 in the angular one, and the reference solution corresponds to N=2000. We also compute  $\mathcal{E}_N$  along the pole removing the contribution of the surface (orange dashed line with square points), which indicates that the surface discontinuity is the dominant source of error and not the hadron-quark interface.

oughly tested for polytropic and hadronic EOSs, the presence of a sharp phase transition boundary may adversely affect convergence. To quantify the effects on convergence by the EOSs considered in this study, we focus on the most massive spheroidal configuration for the equation of state A5 (see table 3) as a representative model of hybrid rotating stars. As a metric for assesing self-convergence, we consider the maximum of the relative difference in energy density profiles with respect to a reference high-resolution

solution. In other words, we compute

$$\mathcal{E}_N = \max \frac{|\epsilon_{\text{ref}}(r,\theta) - \epsilon_N(r,\theta)|}{\epsilon_{\text{ref}}(r,\theta)},$$
 (B.1)

where  $\epsilon_N$  is the energy density computed with N (N/2) radial (angular) points, and  $\epsilon_{\rm ref}$  the reference solution, which we take here to be that at a resolution N=2000. The maximum in eq. (B.1) is evaluated separately along the meridional direction at constant radius  $0.31\,r_p$  and the radial one along the north pole. These constant radius and constant angle lines are chosen such that the corresponding energy density profiles include the phase transition jump, *i.e.*, they cross the interface between the quark and hadronic phases. We also compare  $\mathcal{E}_N$  as computed along a radial direction but without including the contribution from the surface of the star. To do so, we exclude radii with  $r/r_p \gtrsim 0.83$  from the computation of  $\epsilon_N$ , but such that the remaining set of points includes the phase transition.

Figure 15 shows  $\mathcal{E}_N$  for N in the range (200, 1600). The density profiles converge toward the reference solution at similar rates (for  $N \leq 600$ ) regardless of whether we fix the angle or the radius (orange and teal lines) indicating good self-convergence properties. For N > 600 the global solution convergence reaches a plataeu, but  $\mathcal{E}_N$  remains small, and at the level of 1 part in  $10^4$ . As a result of the small value of  $\mathcal{E}_N$ , we find that the global stellar properties (rest mass, gravitational mass and angular momentum) are well-behaved and converged to better than one part in 10<sup>4</sup> for the set of resolutions considered. Finally, the convergence without the contribution from the surface (orange dashed lines in fig. 15) is better than when considering the entire star. This result suggests that the error is dominated by the surface discontinuity, and not by the phase transition.

In our main study we employed a grid with 500 radial points. Based on the convergence study presented here, we estimate that the stellar global properties we report in the main text have an error of  $\sim 0.01\%$ .

# References

- P. Haensel, B. Pichon, Astron. Astrophys. 283, 313 (1994) arXiv:nucl-th/9310003.
- P. Haensel, A.Y. Potekhin, D.G. Yakovlev (Editors), Neutron Stars 1: Equation of State and Structure, Astrophysics and Space Science Library, Vol. 326 (Springer, New York, NY, 2007).
- J.M. Lattimer, Annu. Rev. Nucl. Part. Sci. 62, 485 (2012) arXiv:1305.3510.
- H. Heiselberg, V. Pandharipande, Annu. Rev. Nucl. Part. Sci. 50, 481 (2000) arXiv:astro-ph/0003276.
- J.M. Lattimer, M. Prakash, Astrophys. J. 550, 426 (2001) arXiv:astro-ph/0002232.
- K. Hebeler, J.M. Lattimer, C.J. Pethick, A. Schwenk, Astrophys. J. 773, 11 (2013) arXiv:1303.4662.
- J.M. Lattimer, M. Prakash, Phys. Rep. 621, 127 (2016) arXiv:1512.07820.

- F. Özel, P. Freire, Annu. Rev. Astron. Astrophys. 54, 401 (2016) arXiv:1603.02698.
- J.M. Lattimer, M. Prakash, Phys. Rep. 442, 109 (2007) arXiv:astro-ph/0612440.
- LIGO Scientific Collaboration and Virgo Collaboration, Phys. Rev. Lett. 119, 161101 (2017).
- B.P. Abbott, R. Abbott, T.D. Abbott, F. Acernese, K. Ackley, C. Adams et al., Astrophys. J. Lett. 848, L12 (2017) arXiv:1710.05833.
- B.P. Abbott, R. Abbott, T.D. Abbott, F. Acernese, K. Ackley, C. Adams *et al.*, Astrophys. J. Lett. **848**, L13 (2017) arXiv:1710.05834.
- M. Ajello, A. Allafort, M. Axelsson, L. Baldini, G. Barbiellini, M.G. Baring et al., Astrophys. J. 861, 85 (2018).
- S. Valenti, David, J. Sand, S. Yang, E. Cappellaro, L. Tartaglia et al., Astrophys. J. Lett. 848, L24 (2017) arXiv:1710.05854.
- V. Savchenko, C. Ferrigno, E. Kuulkers, A. Bazzano, E. Bozzo, S. Brandt *et al.*, Astrophys. J. Lett. **848**, L15 (2017) arXiv:1710.05449.
- A. Bauswein, O. Just, H.-T. Janka, N. Stergioulas, Astrophys. J. Lett. 850, L34 (2017) arXiv:1710.06843.
- M. Shibata, S. Fujibayashi, K. Hotokezaka, K. Kiuchi, K. Kyutoku, Y. Sekiguchi *et al.*, Phys. Rev. D **96**, 123012 (2017) arXiv:1710.07579.
- B. Margalit, B.D. Metzger, Astrophys. J. Lett. 850, L19 (2017) arXiv:1710.05938.
- E. Annala, T. Gorda, A. Kurkela, A. Vuorinen, Phys. Rev. Lett. 120, 172703 (2018) arXiv:1711.02644.
- M. Ruiz, S.L. Shapiro, A. Tsokaros, Phys. Rev. D 97, 021501 (2018) arXiv:1711.00473.
- D. Radice, A. Perego, F. Zappa, S. Bernuzzi, Astrophys. J. Lett. 852, L29 (2018) arXiv:1711.03647.
- B.P. Abbott, R. Abbott, T.D. Abbott, F. Acernese, K. Ackley, C. Adams *et al.*, Phys. Rev. Lett. **121**, 161101 (2018) arXiv:1805.11581.
- C.A. Raithel, F. Özel, D. Psaltis, Astrophys. J. Lett. 857, L23 (2018) arXiv:1803.07687.
- E.R. Most, L.R. Weih, L. Rezzolla, J. Schaffner-Bielich, Phys. Rev. Lett. 120, 261103 (2018) arXiv:1803.00549.
- L. Rezzolla, E.R. Most, L.R. Weih, Astrophys. J. Lett. 852, L25 (2018) arXiv:1711.00314.
- G.F. Burgio, A. Drago, G. Pagliara, H.-J. Schulze, J.-B. Wei, Astrophys. J. 860, 139 (2018).
- S. Köppel, L. Bovard, L. Rezzolla, Astrophys. J. Lett. 872, L16 (2019) arXiv:1901.09977.
- C.A. Raithel, Constraints on the Neutron Star Equation of State from GW170817 arXiv:1904.10002.
- M. Alford, A. Sedrakian, Phys. Rev. Lett. 119, 161104 (2017) arXiv:1706.01592.
- 30. U.H. Gerlach, Phys. Rev. **172**, 1325 (1968).
- 31. B. Kampfer, J. Phys. A Math. Gen. 14, L471 (1981).
- 32. K. Schertler, C. Greiner, M.H. Thoma, Nucl. Phys. A **616**, 659 (1997) arXiv:hep-ph/9611305.
- K. Schertler, C. Greiner, P.K. Sahu, M.H. Thoma, Nucl. Phys. A 637, 451 (1998) arXiv:astro-ph/9712165.
- K. Schertler, C. Greiner, J. Schaffner-Bielich, M.H. Thoma, Nucl. Phys. A 677, 463 (2000) arXiv:astroph/0001467.
- N.K. Glendenning, C. Kettner, Astron. Astrophys. 353, L9 (2000) arXiv:astro-ph/9807155.
- 36. N.S. Ayvazyan, G. Colucci, D.H. Rischke, A. Sedrakian, Astron. Astrophys. **559**, A118 (2013) arXiv:1308.3053.

- D. Blaschke, D.E. Alvarez-Castillo, S. Benic, Mass-radius constraints for compact stars and a critical endpoint, arXiv:1310.3803 (2013).
- 38. S. Benić, D. Blaschke, D.E. Alvarez-Castillo, T. Fischer, S. Typel, Astron. Astrophys. **577**, A40 (2015) arXiv:1411.2856.
- P. Haensel, M. Bejger, M. Fortin, L. Zdunik, Eur. Phys. J. A 52, 59 (2016) arXiv:1601.05368.
- M. Bejger, D. Blaschke, P. Haensel, J.L. Zdunik, M. Fortin, Astron. Astrophys. 600, A39 (2017) arXiv:1608.07049.
- M.A.R. Kaltenborn, N.-U.F. Bastian, D.B. Blaschke, Phys. Rev. D 96, 056024 (2017) arXiv:1701.04400.
- D.E. Alvarez-Castillo, D.B. Blaschke, Phys. Rev. C 96, 045809 (2017) arXiv:1703.02681.
- V. Abgaryan, D. Alvarez-Castillo, A. Ayriyan,
   D. Blaschke, H. Grigorian, Universe 4, 94 (2018) arXiv:1807.08034.
- 44. K. Maslov, N. Yasutake, A. Ayriyan, D. Blaschke, H. Grigorian, T. Maruyama et al., Hybrid equation of state with pasta phases and third family of compact stars I: Pasta phases and effective mixed phase model, arXiv:1812.11889 (2018).
- D. Blaschke, N. Chamel, Phases of Dense Matter in Compact Stars, in Astrophysics and Space Science Library, edited by L. Rezzolla, P. Pizzochero, D.I. Jones, N. Rea, I. Vidaña, Astrophysics and Space Science Library, Vol. 457 (Springer, Cham, 2018) p. 337 arXiv:1803.01836.
- D.E. Alvarez-Castillo, D.B. Blaschke, A.G. Grunfeld, V.P. Pagura, Phys. Rev. D 99, 063010 (2019) arXiv:1805.04105.
- V. Paschalidis, K. Yagi, D. Alvarez-Castillo, D.B. Blaschke, A. Sedrakian, Phys. Rev. D 97, 084038 (2018) arXiv:1712.00451.
- A. Drago, G. Pagliara, Astrophys. J. Lett. 852, L32 (2018) arXiv:1710.02003.
- S. Han, A.W. Steiner, Phys. Rev. D 99, 083014 (2019) arXiv:1810.10967.
- Y. Chen, M. Huang, Q.-S. Yan, JHEP 5, 178 (2018) arXiv:1712.03470.
- M. Hanauske, L. Bovard, J. Astrophys. Astron. 39, 45 (2018).
- E. Annala, T. Gorda, A. Kurkela, J. Nättilä, A. Vuorinen, Quark-matter cores in neutron stars, arXiv:1903.09121 (2019).
- E.R. Most, L.J. Papenfort, V. Dexheimer, M. Hanauske,
   S. Schramm, H. Stöcker *et al.*, Phys. Rev. Lett. **122**,
   061101 (2019) arXiv:1807.03684.
- A. Bauswein, N.-U.F. Bastian, D.B. Blaschke, K. Chatziioannou, J.A. Clark, T. Fischer *et al.*, Phys. Rev. Lett. **122**, 061102 (2019) arXiv:1809.01116.
- R. De Pietri, A. Drago, A. Feo, G. Pagliara, M. Pasquali,
   S. Traversi et al., Merger of compact stars in the two-families scenario, arXiv:1904.01545.
- G. Montaña, L. Tolós, M. Hanauske, L. Rezzolla, Phys. Rev. D 99, 103009 (2019) arXiv:1811.10929.
- 57. R.C. Tolman, Proc. Natl. Acad. Sci. 20, 169 (1934).
- J.R. Oppenheimer, G.M. Volkoff, Phys. Rev. 55, 374 (1939).
- 59. J.L. Friedman, J.R. Ipser, Astrophys. J. 314, 594 (1987).
- G.B. Cook, S.L. Shapiro, S.A. Teukolsky, Astrophys. J. 422, 227 (1994).

- Y. Eriguchi, I. Hachisu, K. Nomoto, Mon. Not. R. Astron. Soc. 266, 179 (1994).
- V. Paschalidis, N. Stergioulas, Liv. Rev. Relativ. 20, 7 (2017) arXiv:1612.03050.
- G.B. Cook, S.L. Shapiro, S.A. Teukolsky, Astrophys. J. 424, 823 (1994).
- J.-P. Lasota, P. Haensel, M.A. Abramowicz, Astrophys. J. 456, 300 (1996) arXiv:astro-ph/9508118.
- I.A. Morrison, T.W. Baumgarte, S.L. Shapiro, Astrophys. J. 610, 941 (2004) arXiv:astro-ph/0401581.
- C. Breu, L. Rezzolla, Mon. Not. R. Astron. Soc. 459, 646 (2016) arXiv:1601.06083.
- E. Gourgoulhon, P. Haensel, R. Livine, E. Paluch, S. Bonazzola, J.-A. Marck, Astron. Astrophys. 349, 851 (1999) arXiv:astro-ph/9907225.
- D. Gondek-Rosińska, T. Bulik, L. Zdunik, E. Gourgoulhon, S. Ray, J. Dey et al., Astron. Astrophys. 363, 1005 (2000) arXiv:astro-ph/0007004.
- S. Bhattacharyya, I. Bombaci, D. Logoteta, A.V. Thampan, Mon. Not. R. Astron. Soc. 457, 3101 (2016) arXiv:1601.06120.
- G.B. Cook, S.L. Shapiro, S.A. Teukolsky, Astrophys. J. 398, 203 (1992).
- T.W. Baumgarte, S.L. Shapiro, M. Shibata, Astrophys. J. Lett. 528, L29 (2000) arXiv:astro-ph/9910565.
- P.L. Espino, V. Paschalidis, Phys. Rev. D 99, 083017 (2019) arXiv:1901.05479.
- L. Baiotti, L. Rezzolla, Rep. Prog. Phys. 80, 096901 (2017) arXiv:1607.03540.
- V. Paschalidis, Class. Quantum Grav. 34, 084002 (2017) arXiv:1611.01519.
- M. Ansorg, D. Gondek-Rosińska, L. Villain, Mon. Not. R. Astron. Soc. 396, 2359 (2009).
- A.M. Studzińska, M. Kucaba, D. Gondek-Rosińska, L. Villain, M. Ansorg, Mon. Not. R. Astron. Soc. 463, 2667 (2016).
- 77. D. Gondek-Rosińska, I. Kowalska, L. Villain, M. Ansorg, M. Kucaba, Astrophys. J. **837**, 58 (2017) arXiv:1609.02336.
- E. Zhou, A. Tsokaros, K. Uryu, R. Xu, M. Shibata, Differentially rotating strange star in general relativity, arXiv:1902.09361 (2019).
- M. Szkudlarek, D. Gondek-Rosińska, L. Villain, M. Ansorg, Maximum Mass of Differentially Rotating Strange Quark Stars, arXiv:1904.03759 (2019).
- 80. P. Espino, V. Paschalidis, T. Baumgarte, S.L. Shapiro, On the Dynamical Stability of Quasi-Toroidal Neutron Stars, arXiv:1906.08786 (2019).
- H. Komatsu, Y. Eriguchi, I. Hachisu, Mon. Not. R. Astron. Soc. 237, 355 (1989).
- H. Komatsu, Y. Eriguchi, I. Hachisu, Mon. Not. R. Astron. Soc. 239, 153 (1989).
- K. Yagi, N. Yunes, Phys. Rev. D 88, 023009 (2013) arXiv:1303.1528.
- 84. K. Yagi, N. Yunes, Science **341**, 365 (2013) arXiv:1302.4499.
- K. Yagi, L.C. Stein, G. Pappas, N. Yunes, T.A. Apostolatos, Phys. Rev. D 90, 063010 (2014) arXiv:1406.7587.
- 86. K. Yagi, N. Yunes, Phys. Rep. **681**, 1 (2017) arXiv:1608.02582.
- 87. D. Bandyopadhyay, S.A. Bhat, P. Char, D. Chatterjee, Eur. Phys. J. A **54**, 26 (2018) arXiv:1712.01715.

- G. Pappas, T.A. Apostolatos, Phys. Rev. Lett. 112, 121101 (2014) arXiv:1311.5508.
- S. Chakrabarti, T. Delsate, N. Gürlebeck, J. Steinhoff, Phys. Rev. Lett. 112, 201102 (2014) arXiv:1311.6509.
- G. Bozzola, N. Stergioulas, A. Bauswein, Mon. Not. R. Astron. Soc. 474, 3557 (2018) arXiv:1709.02787.
- J.L. Friedman, J.R. Ipser, R.D. Sorkin, Astrophys. J. 325, 722 (1988).
- K. Takami, L. Rezzolla, S. Yoshida, Mon. Not. R. Astron. Soc. 416, L1 (2011) arXiv:1105.3069.
- A. Bauswein, N. Stergioulas, Mon. Not. R. Astron. Soc. 471, 4956 (2017) arXiv:1702.02567.
- L.R. Weih, E.R. Most, L. Rezzolla, Mon. Not. R. Astron. Soc. 473, L126 (2018) arXiv:1709.06058.
- G. Baym, C. Pethick, P. Sutherland, Astrophys. J. 170, 299 (1971).
- J.W. Negele, D. Vautherin, Nucl. Phys. A 207, 298 (1973).
- 97. G. Colucci, A. Sedrakian, Phys. Rev. C **87**, 055806 (2013) arXiv:1302.6925.
- 98. P. Ring, J. Phys. Conf. Ser. 205, 012010 (2010).
- G.A. Lalazissis, T. Nikšić, D. Vretenar, P. Ring, Phys. Rev. C 71, 024312 (2005).
- 100. E. Witten, Phys. Rev. D 30, 272 (1984).
- P. Haensel, J.L. Zdunik, R. Schaefer, Astron. Astrophys. 160, 121 (1986).
- C. Alcock, E. Farhi, A. Olinto, Astrophys. J. 310, 261 (1986).
- J.L. Zdunik, Astron. Astrophys. 359, 311 (2000) arXiv:astro-ph/0004375.
- 104. Z.F. Seidov, Sov. Astron. 15, 347 (1971).
- J.L. Zdunik, P. Haensel, Astron. Astrophys. 551, A61 (2013) arXiv:1211.1231.
- M.G. Alford, S. Han, M. Prakash, JPS Conf. Proc. 1, 013041 (2014).
- J.S. Read, B.D. Lackey, B.J. Owen, J.L. Friedman, Phys. Rev. D 79, 124032 (2009).

- 108. C.A. Raithel, F. Özel, D. Psaltis, Astrophys. J. 831, 44 (2016) arXiv:1605.03591.
- L. Bonanno, A. Sedrakian, Astron. Astrophys. 539, A16 (2012) arXiv:1108.0559.
- 110. P.B. Demorest, T. Pennucci, S.M. Ransom, M.S.E. Roberts, J.W.T. Hessels, Nature **467**, 1081 (2010) arXiv:1010.5788.
- J. Antoniadis, P.C.C. Freire, N. Wex, T.M. Tauris, R.S. Lynch, M.H. van Kerkwijk *et al.*, Science **340**, 1233232 (2013).
- E. Fonseca, T.T. Pennucci, J.A. Ellis, I.H. Stairs, D.J. Nice, S.M. Ransom *et al.*, Astrophys. J. **832**, 167 (2016) arXiv:1603.00545.
- Z. Arzoumanian, A. Brazier, S. Burke-Spolaor, S. Chamberlin, S. Chatterjee, B. Christy et al., Astrophys. J. Suppl. 235, 37 (2018) arXiv:1801.01837.
- 114. H. Cromartie, E. Fonseca, S.M. Ransom, P.B. Demorest, Z. Arzoumanian, H. Blumer et al., A very massive neutron star: relativistic Shapiro delay measurements of PSR J0740+6620, arXiv:1904.06759 (2019).
- J.M. Bardeen, R.V. Wagoner, Astrophys. J. 167, 359 (1971).
- 116. J.L. Friedman, N. Stergioulas, *Rotating Relativistic Stars* (Cambridge University Press, 2013).
- 117. R.D. Sorkin, Astrophys. J. 257, 847 (1982).
- J.S. Schiffrin, R.M. Wald, Class. Quantum Grav. 31, 035024 (2014) arXiv:1310.5117.
- K. Prabhu, J.S. Schiffrin, R.M. Wald, Class. Quantum Grav. 33, 185007 (2016) arXiv:1606.00859.
- N. Stergioulas, J.L. Friedman, Astrophys. J. 444, 306 (1995) arXiv:astro-ph/9411032.
- 121. T. Nozawa, N. Stergioulas, E. Gourgoulhon, Y. Eriguchi, Astron. Astrophys. Suppl. **132**, 431 (1998) arXiv:gr-qc/9804048.
- R. Pordes, OSG Consortium, D. Petravick, B. Kramer,
   D. Olson, M. Livny et al., J. Phys. Conf. Ser. 78, 012057 (2007).